



Texas Water Journal

Volume 14 Number 1 | 2023





Texas Water Journal

Volume 14, Number 1

2023

ISSN 2160-5319

texaswaterjournal.org

THE TEXAS WATER JOURNAL is an online, peer-reviewed, and indexed journal devoted to the timely consideration of Texas water resources management, research, and policy issues. The journal provides in-depth analysis of Texas water resources management and policies from a multidisciplinary perspective that integrates science, engineering, law, planning, and other disciplines. It also provides updates on key state legislation and policy changes by Texas administrative agencies.

For more information on the Texas Water Journal as well as our policies and submission guidelines, please visit texaswaterjournal.org. As a 501(c)(3) nonprofit organization, the Texas Water Journal needs your support to provide Texas with an open-accessed, peer-reviewed publication that focuses on Texas water. Please consider [donating](#).

Editor-in-Chief

Todd H. Votteler, Ph.D.
Collaborative Water Resolution LLC

Managing Editor

Vacant

Layout Editor

Sarah L. Richardson
Texas Water Resources Institute

Editorial Board

Kathy A. Alexander, Ph.D.
Texas Commission on Environmental Quality

Jude A. Benavides, Ph.D.
The University of Texas, Rio Grande Valley

Gabriel B. Collins, J.D.
Baker Institute for Public Policy

Nelun Fernando, Ph.D.
Texas Water Development Board

Ken Kramer, Ph.D.
Lone Star Chapter of the Sierra Club

Dorina Murgulet, Ph.D.
Texas A&M University-Corpus Christi

Ken A. Rainwater, Ph.D.
Texas Tech University

Rosario F. Sanchez, Ph.D.
Texas Water Resources Institute

Michael H. Young, Ph.D.
The University of Texas at Austin



The Texas Water Journal is published in cooperation with the Texas Water Resources Institute, part of Texas A&M AgriLife Research, the Texas A&M AgriLife Extension Service, and the College of Agriculture and Life Sciences at Texas A&M University and the Bureau of Economic Geology in the Jackson School of Geosciences at The University of Texas at Austin.



The Texas Water Journal is indexed by [Scopus](#), [Google Scholar](#), and the [Directory of Open Access Journals](#).

Cover photo:

Santa Elena Canyon, Big Bend National Park, Texas.

©2022 Rob Doyle, Pluto911 Photography

Discrete Streamflow Measurements and Waterborne Self-Potential Logging of a 43-Kilometer-Long Reach of the Elm Fork Trinity River Upstream from Dallas, Texas

Jonathan V. Thomas¹, Scott J. Ikard², Roger K. Trader¹, David Rodriguez¹

Abstract: Continuous and discrete streamflow data were combined with waterborne self-potential, surface-water temperature, and surface-water conductivity surveys obtained along an approximately 43-kilometer (26.7 mile) surveyed reach of the Elm Fork Trinity River (hereinafter referred to as “Elm Fork”) upstream from Dallas, Texas, to investigate areas of gaining and losing streamflow under various streamflow and seasonal climatic conditions. Discrete streamflow measurements were made at 17 locations on October 12, 2021, and January 25, 2022, at 19 locations on May 17, 2022, and at 18 locations on August 9, 2022. Waterborne self-potential data were measured from a kayak in January 2022 during a period of base flow along three individually surveyed reaches between the Lake Lewisville Dam and Frasier Dam on the Elm Fork. Together, these data indicated different parts of the Elm Fork functioned as either a gaining or losing stream depending on streamflow and seasonal climatic conditions. Overall, there were estimated net gains in streamflow during the first two discrete-measurement events of about 107 and 2 cubic feet per second in October 2021 and January 2022, respectively, and estimated net losses in streamflow in May 2022 and August 2022 of about 24 and 18 cubic feet per second, respectively.

Keywords: Gain, Loss, Trinity River, Elm Fork, Dallas

¹ U.S. Geological Survey, Oklahoma-Texas Water Science Center, Fort Worth, Texas

² U.S. Geological Survey, Oklahoma-Texas Water Science Center, Austin, Texas

* Corresponding author: jvrthomas@usgs.gov

Received 29 March 2023, Accepted 19 June 2023, Published online 16 August 2023.

Citation: Thomas JV, Ikard SJ, Trader RK, Rodriguez D. 2023. Discrete Streamflow Measurements and Waterborne Self-Potential Logging of a 43-Kilometer-Long Reach of the Elm Fork Trinity River Upstream from Dallas, Texas. *Texas Water Journal*. 14(1):81-104. Available from: <https://doi.org/10.21423/twj.v14i1.7158>.

© 2023 Jonathan V. Thomas, Scott J. Ikard, Roger K. Trader, and David Rodriguez. This work is licensed under the Creative Commons Attribution 4.0 International License. To view a copy of this license, visit <https://creativecommons.org/licenses/by/4.0/> or visit the TWJ [website](#).

Terms used in paper

| Acronym/Initialism | Descriptive Name |
|--------------------|------------------------------------|
| °C | degrees Celsius |
| ADCP | acoustic Doppler current profilers |
| ADV | acoustic doppler velocimeters |
| C/m ³ | cubic meters |
| C/m ³ | coulombs per cubic meter |
| CST | Central Standard Time |
| DWU | Dallas Water Utilities |
| ft ³ /s | cubic feet per second |
| GW | groundwater |
| Hz | hertz |
| km | kilometer |
| m | meters |
| m/m | meters per meter |
| m/s | meters per second |
| m ² | square meters |
| mv | millivolts |
| mV/m | millivolts per meter |
| NWIS | National Water Information System |
| ohm-m | ohm meters |
| s | seconds |
| SP | spontaneous potential |
| SW | surface water |
| TRAA | Trinity River alluvium aquifer |
| TWDB | Texas Water Development Board |
| USGS | U.S. Geological Survey |
| WaSP | waterborne self-potential |
| WTP | water treatment plant |
| μS/cm | microsiemens per centimeter |

INTRODUCTION

Dallas Water Utilities (DWU) is a primary supplier of water to more than 2.5 million people in north Texas ([Dallas Water Utilities, 2019](#)). To meet the increasing water demands of a growing population, DWU has developed a water-conservation plan to reduce consumptive losses and increase water reuse within their service area ([Dallas Water Utilities, 2019](#)). Additionally, DWU has constructed reservoirs and infrastructure to procure and manage water resources and to augment surface-water (SW) diversions from the Elm Fork Trinity River (hereinafter referred to as “Elm Fork”). A better understanding of streamflow gains and losses in the Elm Fork would help to inform DWU’s water conservation plan. Hence, the U.S. Geological Survey (USGS) in cooperation with DWU characterized possible gaining and losing reaches of the Elm Fork during different streamflow conditions between October 2021 and August 2022.

SW and groundwater (GW) are typically managed separately as disconnected resources even though they are indeed a single resource with respect to streams that are hydraulically connected to alluvial aquifers ([Winter and others, 1999](#); [Fuchs and others, 2019](#)). Braun and Grzyb ([2015, p. 1](#)) explain “in the absence of appreciable tributary inflows or diversions of flow out of the channel, the question of whether a given reach gains or loses streamflow depends largely on groundwater/surface-water interactions.” Transfers of water between streams and the Trinity River alluvium aquifer (TRAA), referred to herein as SW-GW exchanges, occur throughout the Trinity River basin and vary spatially and temporally depending on the amount of streamflow ([Slade and others, 2002](#)). During drought periods, streamflows in the Elm Fork are primarily sustained by reservoir releases or base flows from the TRAA. During peak-streamflow periods, recharge to the TRAA occurs as SW flows into the aquifer from the stream. At a given moment, SW gains can occur at one location in the stream, or in a net sense along an arbitrary reach, while SW losses are simultaneously occurring at another location, or in a net sense along a different reach ([McCallum and others, 2013](#)). Quantifying the rates of SW-GW exchange in the Elm Fork is, therefore, challenging because the spatial and temporal dynamics governing SW gains and losses are often unknown and variable ([Sophocleous, 2002](#); [Kalbus and others, 2006](#)).

Traditional hydrologic methods such as discrete streamflow measurements provide low spatial and temporal resolution of the SW-GW exchanges that they seek to quantify and generally only indicate the net gain or loss along a given reach for practical purposes. In contrast, continuous streamflow data computed at USGS streamgages provide better temporal resolution of streamflow variability at specific stream locations but provide limited spatial resolution because they can only indicate net quantities of SW gain or loss between streamgages. Alternative-

ly, waterborne self-potential (WaSP) surveys enable mapping of SW-GW exchanges over stream reaches that vary in length from a few meters (m) to hundreds of kilometers or more. WaSP surveys have been used to identify distributed reach-scale and hyporheic-scale exchanges ([Ikard and others, 2018](#); [Ikard and others, 2021b](#)), as well as focused exchanges in specific sections of a reach ([Ikard and others, 2021a](#)); however, as with any geophysical method, WaSP surveys require auxiliary geophysical, geochemical, or hydraulic data to infer locations and quantities of gain or loss. Combining continuous streamflow data and discrete streamflow measurements with WaSP surveys provides an enhanced methodology to better understand SW-GW exchanges distributed over long stream reaches and the relative magnitudes of the exchange rates between locations where continuous and discrete streamflow measurements are acquired.

This article describes gaining and losing reaches of the Elm Fork that were assessed between Lake Lewisville Dam and Frasier Dam, upstream from Dallas, Texas (Figure 1). During the study, continuous streamflow and discrete streamflow measurements were obtained at five continuous USGS streamgages and 14 discrete streamflow measurement sites. Three of the streamgages were on the main stem of the Elm Fork and two were on tributaries to the Elm Fork. Streamflow data were combined with WaSP survey data obtained along a 43-kilometer (km) long (26.7 mile) surveyed reach of the Elm Fork between Lake Lewisville Dam and Frasier Dam. Streamflow measurements were made multiple times between October 2021 and August 2022 and supplemented by the WaSP survey in January 2022.

DESCRIPTION OF THE STUDY AREA

The Elm Fork is one of four main tributaries that form the Trinity River (Figure 1). The Trinity River flows from its headwaters in north-central Texas north of the Dallas-Fort Worth metropolitan area southeastward for approximately 885 km (550 miles) before emptying into the Gulf of Mexico east of Houston, Texas ([Texas Water Development Board, 2019](#)). Four main tributaries (Clear Fork, East Fork, Elm Fork, and West Fork Trinity River) converge in the Dallas-Fort Worth metropolitan area to form the main stem of the Trinity River ([Trinity River Authority, 2021](#)). The main stem of the Trinity River conveys the third largest average annual streamflow volume of all major rivers in Texas; the average annual streamflow estimated by the Texas Water Development Board (TWDB) is about 5,727,000 acre-feet per year ([Texas Water Development Board, 2019](#)). The Trinity River currently (2023) provides water to an estimated 14 million people—slightly less than half of the entire Texas population of about 30 million in 2022 ([U.S. Census Bureau, 2023](#))—and the number of people that will rely on Trinity River water is projected to increase to 25.7 million by 2070 ([Trinity River Authority, 2021](#)).

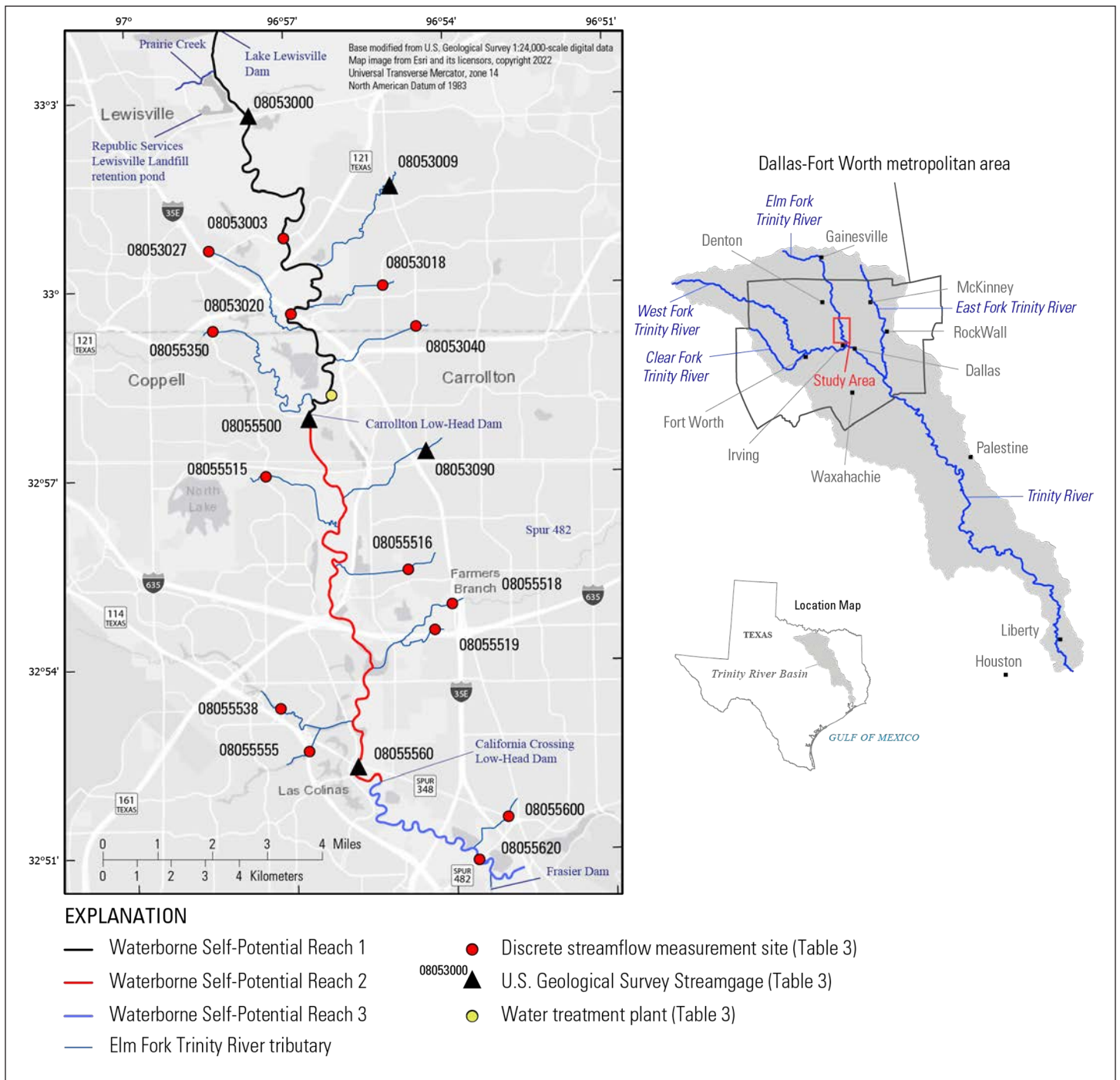


Figure 1. Location map showing discrete streamflow measurement sites, continuous streamgages, waterborne self-potential reaches, and a water treatment plant (WTP) in the study area of the Elm Fork Trinity River between Lake Lewisville Dam and Frasier Dam in the Dallas-Fort Worth metropolitan area.

The Trinity River has carved its main floodplain into the underlying sediments. Carved out fluvial valleys are now infilled by five terraced alluvial units, distinguishable according to their elevation above the streambed ([Allen and Flanigan, 1986](#)). The lithology of the terraces varies from sand and gravel to sandy loams to scattered pebbles and cobbles of quartzite at the highest elevations above the floodplain ([Allen and Flanigan, 1986](#)). The TWDB does not recognize the Trinity River alluvium aquifer as a major or minor aquifer of Texas, although Groundwater Management Area 14, the Region H Water Planning Group, and Bluebonnet Groundwater Conservation District all recognize the TRAA as a viable aquifer ([Williams, 2010](#); [Groundwater Management Area 14, 2016](#); [Region H Water Planning Group, 2021](#)). According to the Bluebonnet Groundwater Conservation District's GW management plan, there is little published information on the composition and hydraulic properties of the aquifer, although it is likely to have similar composition and texture as the Brazos River alluvial aquifer and is described generally as alluvium and broad fluvial terrace deposits of silts and fine-grained sands and gravels of Quaternary age ([Coffman and others, 2011](#); [U.S. Geological Survey, 2014](#)). The TRAA was formed by incision of the Trinity River and its tributaries as a result of increased rainfall and streamflow within the basin during the Pleistocene ([Stern, 2019](#)). [Allen and Flanigan \(1986\)](#) describe the alluvium of the present-day floodplains and terraces as varying between silty clays, impervious to semi-pervious clays, clayey sands, and gravel lenses, and indicate that the thickness of the TRAA varies from 1.5–4.6 m on small tributaries to 17–27 m on the major streams and main stem ([Allen and Flanigan, 1986](#)). An analysis from more than 1,000 geotechnical driller's logs has identified that at least four levels of terraced deposits are present in the downtown Dallas central business district ranging in thickness from 3.1–10.7 m and are primarily composed of silty clays, clays, and silty sands with interspersed sand and gravel lenses ([Allen and Flanigan, 1986](#)). These alluvium and terrace geologic units are hydraulically connected to the present-day Trinity River and its tributaries.

Within the Dallas Fort Worth metropolitan area, the humid subtropical climate is characterized by hot summers and wide annual temperature ranges; sporadic large thunderstorms are common ([National Weather Service, 2023a](#)). Likewise, precipitation varies considerably, where annual values range from less than 20 inches to more than 50 inches and is unevenly distributed throughout the year, typically favoring a bimodal distribution of wet spring/fall and dry summer/winter ([National Weather Service, 2023a](#)).

METHODS

Because the spatial and temporal dynamics governing SW gains and losses in the reach of the Elm Fork between Lake

Lewisville Dam and Frasier Dam are not well understood, a combination of methods were used to improve the understanding of the complex nature of SW and GW interactions in this reach. The objective was to better understand streamflow gains and losses by (1) assessing existing continuous streamflow data from select USGS streamgages, (2) collecting discrete streamflow measurements at select streamgages over four discrete-measurement events, and (3) measuring and logging continuous surveys of WaSP, SW temperature, and specific conductance along each WaSP reach of the Elm Fork.

Streamflow Measurements

This study combined continuous streamflow data from USGS streamgages, discrete streamflow measurements on the main stem of the Elm Fork and its tributaries, and a WaSP survey of streamflow gains and losses in three reaches on the main stem of the Elm Fork (Figure 1). Discrete streamflow measurements were made at 17 locations on October 12, 2021 and January 25, 2022, at 19 locations on May 17, 2022, and at 18 locations on August 9, 2022. Each streamflow measurement location is shown on Figure 1. In total, 65 discrete streamflow measurements were made consisting of 23 acoustic Doppler current profilers (ADCP) streamflow measurements and 42 acoustic doppler velocimeters (ADV) streamflow measurements; there were also six observations of no flow. The methods used to measure streamflow are described in [Turnipseed and Sauer \(2010\)](#) and [Mueller and others \(2013\)](#). Each discrete streamflow measurement was assigned a measurement rating by a hydrographer (excellent, good, fair, or poor) representing different estimated uncertainty ranges; the uncertainty ranges are assigned using both quantitative and qualitative guidelines as described in [Turnipseed and Sauer \(2010\)](#) and [Mueller and others \(2013\)](#). For this study, the assigned uncertainty for a given measurement ranged from 5 percent for a measurement rated as good to 10 percent for a measurement rated as poor and provides context as to how precise additional computations using these values may be considered ([Turnipseed and Sauer, 2010](#)). All discrete streamflow measurements for this study are available from the U.S. Geological Survey National Water Information System (NWIS) ([U.S. Geological Survey, 2023](#)).

Streamflow measurements were completed during a wide range of streamflow conditions, where the inflow at the uppermost site (USGS streamgage 08053000 Elm Fork Trinity River near Lewisville, Texas [hereinafter referred to as "streamgage 08053000"]) varied from 207 to 1,610 ft³/s. In addition to streamgage 08053000, continuous streamflow data were evaluated at two additional USGS streamgages: USGS streamgage 08055500 Elm Fork Trinity River near Carrollton, Texas (hereinafter referred to as "streamgage 08055500"), and USGS streamgage 08055560 Elm Fork Trinity River at

Table 1. Summary of U.S. Geological Survey streamgages and Elm Fork Water Treatment Plant withdrawals in cubic feet per second (ft³/s) on the Elm Fork Trinity River between Lake Lewisville Dam and Frasier Dam. Statistics include streamflow data for the date of discrete measurements (gray rows) and from 12:00 am Central Standard Time (CST) two days prior to and including the date of the discrete measurements (white rows).

| Date range | Streamflow statistic | USGS streamgage 08053000 Elm Fork Trinity River near Lewisville, Texas | Elm Fork Water Treatment Plant withdrawals | USGS streamgage 08055500 Elm Fork Trinity River near Carrollton, Texas | USGS streamgage 08055560 Elm Fork Trinity River at Spur 348, Irving, Texas |
|---------------------|----------------------|--|--|--|--|
| | | Elm Fork Trinity River near Carrollton, Texas | | | |
| October 10–12, 2021 | Minimum | 298 | 221 | 124 | 142 |
| | Maximum | 429 | 237 | 851 | 993 |
| | Mean | 320 | 229 | 302 | 406 |
| October 12, 2021 | Mean | 310 | 221 | 210 | 312 |
| January 23–25, 2022 | Minimum | 204 | 182 | 59.0 | 68.0 |
| | Maximum | 214 | 231 | 130 | 112 |
| | Mean | 209 | 204 | 93.2 | 86.7 |
| January 25, 2022 | Mean | 207 | 182 | 107 | 91.8 |
| May 15–17, 2022 | Minimum | 1,610 | 253 | 1,400 | 1,460 |
| | Maximum | 1,670 | 310 | 1,630 | 1,770 |
| | Mean | 1,630 | 281 | 1,530 | 1,580 |
| May 17, 2022 | Mean | 1,610 | 310 | 1,450 | 1,510 |
| August 7–9, 2022 | Minimum | 478 | 351 | 139 | 142 |
| | Maximum | 519 | 382 | 231 | 186 |
| | Mean | 494 | 366 | 173 | 163 |
| August 9, 2022 | Mean | 502 | 363 | 182 | 155 |

Spur 348, Irving, Texas (hereinafter referred to as “streamgage 08055560”) and are summarized in Table 1 for both the day of and two days prior to each discrete-measurement event. The streamgages are depicted in downstream order (Figure 1). Streamflow hydrographs measured at each streamgage from September 1, 2021 to September 30, 2022, and during the survey are shown in Figure 2 beginning at 12:00 am Central Standard Time (CST) two days prior to the discrete-measurement events and ending five days later.

For this article, streamflow gains or losses were estimated by measuring the difference in streamflow at the upstream and downstream extent of each reach while accounting for other sources of gains and losses such as tributary inflow and water supply withdrawals. Gains and losses were calculated as a whole and were not broken out into spring or seep inflow, unidentified return flows, or evaporative losses. Estimates of gains or losses for each reach (between main stem streamflow measurements) were estimated using Equation 1.

$$G = (QD+W) - (QU + T) \tag{1}$$

Estimated gains or losses (*G*) represent a gaining streamflow reach when positive and a losing streamflow reach when negative. For each reach, the upstream streamflow measurement was used for *QU* and the next downstream main stem streamflow measurement was used for *QD*. The water-use withdrawal value (*W*) is representative of the total withdrawals in a reach; however, the only appreciable withdrawal rates relative to the Elm Fork streamflow were made at a water treatment plant (WTP) (Figure 1). Tributary inflow (*T*) was calculated by the sum of all measured tributary inflows to the Elm Fork between *QU* and *QD*.

Waterborne Self-potential Survey

WaSP surveys utilize the physical relation between the electric field (*E*; millivolts per meter [mV/m]) and the electric-potential gradient. An electric field exists in a region of space around an electrically charged object or surface-area such as a streambed (Blakely, 1996; Griffiths, 1999). The electric field is a vector-field whose direction is defined to be the direction of electromotive force exerted on a positive electric charge placed at an arbitrary point within the electric field. The electric field

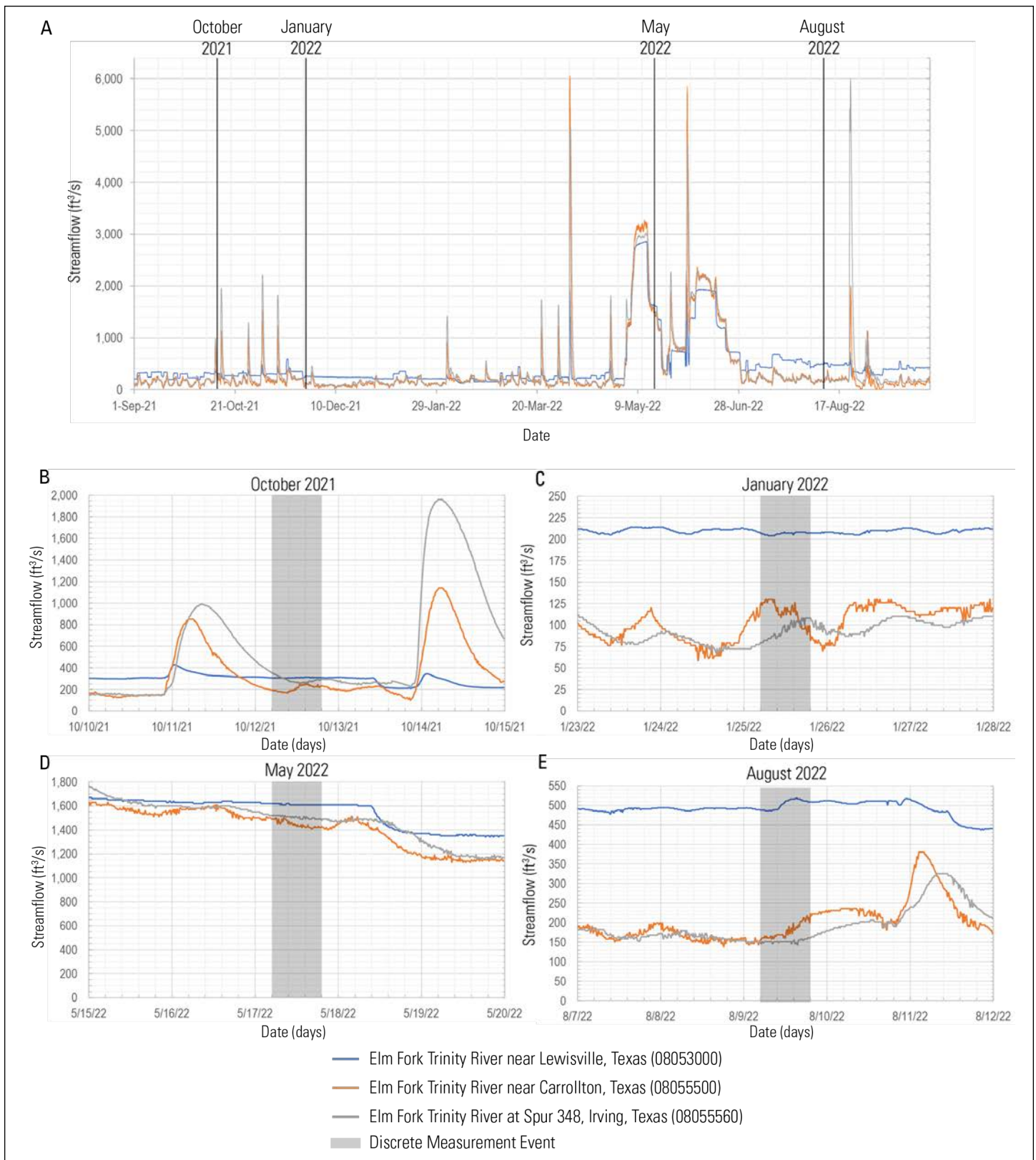


Figure 2. Streamflow in cubic feet per second (ft³/s) in the Elm Fork Trinity River at U.S. Geological Survey streamgages from (A) September 1, 2021 to September 30, 2022 and (B–E) from 12:00 am Central Standard Time (CST) two days prior to and through two days after the date of the discrete-measurement events in (B) October 2021, (C) January 2022, (D) May 2022, and (E) August 2022 between Lake Lewisville Dam and Frasier Dam.

can be derived from the electric potential gradient ($-\nabla\varphi$; mV/m) by Equation 2 where \mathbf{x} (m), \mathbf{y} (m), and \mathbf{z} (m) are unit vectors in the x-, y-, and z-coordinate directions, respectively, and $\partial\varphi/\partial x$, $\partial\varphi/\partial y$ and $\partial\varphi/\partial z$ are partial derivatives of the electric-potential gradient in the x, y, and z directions (Blakely, 1996; Griffiths, 1999).

$$\mathbf{E} = -\nabla\varphi = -\frac{\partial\varphi}{\partial x}\mathbf{x} - \frac{\partial\varphi}{\partial y}\mathbf{y} - \frac{\partial\varphi}{\partial z}\mathbf{z} \quad (2)$$

The vector magnitude of the electric field intensity decreases from regions of high electric potential (φ ; mV) toward regions of low electric potential. Assessing the electric field in one-dimension, the x-coordinate direction (defined herein as the streamflow direction), the partial derivatives in Equation 2 in the y- and z-coordinate directions are neglected and the partial derivative in the x-coordinate direction is expressed as $-\partial\varphi/\partial x = -(\Delta\varphi)/\Delta x$, as shown in Equation 3 where φ_2 and φ_1 are electric potentials at locations x_2 and x_1 , respectively, $\Delta\varphi = (\varphi_2 - \varphi_1)$ (mV) is the potential difference of the two electric potentials, and $\Delta x = (x_2 - x_1)$ (m) is the distance between x_2 and x_1 . Equation 3 indicates that the electric field intensity is calculated as the difference in electric potential between two arbitrary points divided by the distance between the points (Blakely, 1996; Griffiths, 1999).

$$E = -\frac{\Delta\varphi}{\Delta x} = -\frac{(\varphi_2 - \varphi_1)}{(x_2 - x_1)} \quad (3)$$

Electric potential is a measure of energy per unit charge, such that the potential difference between two points is the change in potential energy of an electric charge as it accelerates from position x_2 to position x_1 within the surrounding electric field (Blakely, 1996; Griffiths, 1999). The electric-potential between locations x_2 and x_1 is calculated with Equation 4 as the integral summation of the electric field intensity, where $\varphi(x)$ is the electric potential in the x-coordinate direction between locations x_1 and x_2 (Blakely, 1996; Griffiths, 1999).

$$\varphi(x) = -\int_{x_1}^{x_2} E(x)dx \quad (4)$$

The basic premise of a WaSP survey is that an electric potential in a SW body is calculated from voltage differences that are measured by an electric dipole composed of two non-polarizing electrodes as the dipole traverses the reach. The voltage differences between the positive and negative electrodes of the dipole are measured continuously and logged at a 1-hertz (Hz) frequency as the dipole floats in a downstream x-coordinate direction in the SW with the positive electrode positioned at x_2 downstream from the negative electrode at x_1 , such that the measured voltage difference at each location along the profile is $\Delta\varphi = (\varphi_2 - \varphi_1)$. The locations x_2 and x_1 are updated with each successive measurement, and the distance between them remains constant for every measurement such that Δx is

equal to the dipole length. The measured voltage differences are corrected for transient electrode-drift and topographic effects (Table 2; Figures 3–4) when present (Ernstson and Scherer, 1986; Ikard and others, 2021a), converted into electric field intensity with Equation 5, partitioned into low spatial-frequency (L) and high spatial-frequency (H) data components through digital signal processing (Oppenheim and Schaffer, 2010; Ikard and others, 2018; Ikard and others, 2021b), and subsequently numerically integrated into corresponding L and H electric-potential components. The electric-potential profile is then interpreted to identify apparent gaining and losing stream reaches over different spatial scales by the changes in polarity of the electric potential (Valois and others, 2017; Ikard and others, 2018). In the case of SW-GW exchange, the attributed causes of the electric-potential changes in polarity (gains represented by positive electric-potential values) are streaming-currents generated on the streambed and submerged streambanks by streamflow gains from GW or SW losses into the porous streambed and flood-plain sediments (Ikard and others, 2021b). The data-processing scripts that produce the electric-potential values were published as part of the companion data release (Ikard and others, 2022).

Figures 3B–D show plots of the voltage differences versus the topographic elevation at the location of each measurement. Minor topographic effects are present in WaSP reach 1, shown by the small positive slope of the ordinary least-squares linear regression line fitted to the point cloud of elevation-voltage data in the corresponding scatterplot (Table 2; Figure 3B). There is negligible topographic effect in WaSP reaches 2 and 3, indicated by the approximately horizontal regression lines fitted to the data (Table 2; Figures 3C and D). The topographic effects are described by the slope (m) and y-intercept (b) coefficients of the regression lines that are summarized in Table 2.

$$\Delta V_Z = mz + b \quad (5)$$

$$\Delta V_C = \Delta V - \Delta V_Z \quad (6)$$

Terrain corrections are commonly applied to self-potential data when topographic effects are present. Topographic effects are typically attributed to the downward percolation of GW along hill slopes in areas with topographic relief (Ernstson and Scherer, 1986; Barde-Cabusson and others, 2021) and in that sense are expected to produce a topographic effect characterized by linear increases in measured voltage differences with decreasing elevation (Ernstson and Scherer, 1986). Ikard and others, (2021c) observed the opposite topographic effect where the measured voltage differences increased with increasing elevation. A topographic terrain correction was applied to the measured voltage data obtained from each reach of the Elm Fork by computing a terrain voltage (ΔV_Z ; mV) for each

Table 2. Summary of Equation 5 coefficients of ordinary least-squares linear regression lines used to make terrain corrections to each waterborne self-potential reach data measured in the Elm Fork Trinity River.

| Survey Reach | Eqn. 5 slope coefficient (m; millivolts/meter) | Eqn. 5 intercept coefficient (b; meter) | Coefficient of determination (unitless) |
|--------------|--|---|---|
| 1 | 0.0817 | -9.49 | 0.0668 |
| 2 | -0.0278 | 4.602 | 0.0038 |
| 3 | -0.0322 | 2.987 | 0.0042 |

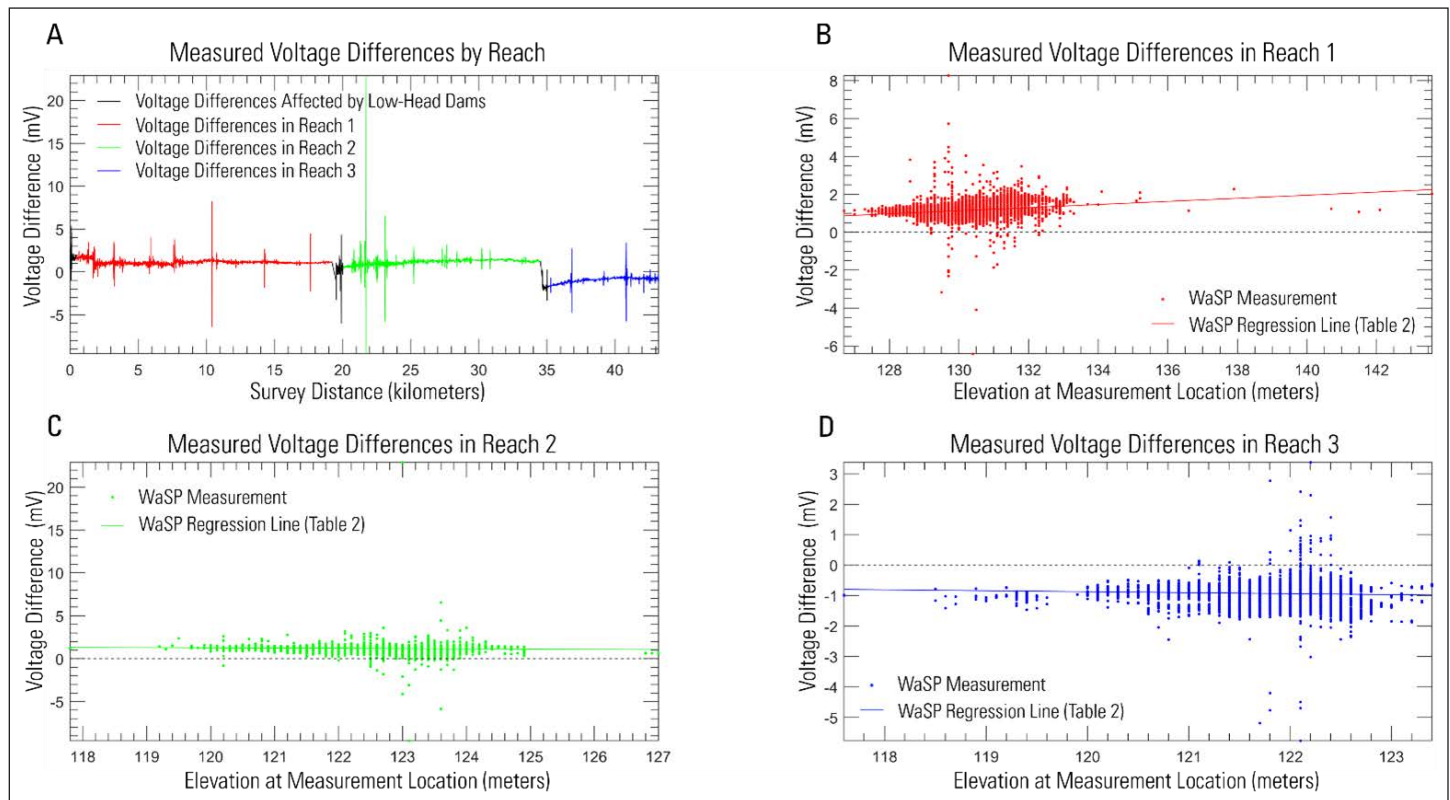


Figure 3. Graph in panel A shows the voltage differences in millivolts (mV) measured along three waterborne self-potential (WaSP) reaches of the Elm Fork Trinity River. Graphs in panels B, C, and D plot voltage differences (mV) versus elevation (meters) along each WaSP reach. In panel A, voltage differences are depicted in black for areas affected by low-head dams and subsequently removed from further consideration (Figure 1).

measurement using Equation 5 and the coefficients in Table 2. Equation 6 is then used to subtract the terrain voltages from the measured voltages to calculate the corrected voltage (ΔV_c ; mV). The effects of the terrain corrections on the measured voltage differences are shown in Figure 4 for each survey reach. After applying terrain corrections, the corrected voltage differences were centered around 0 mV. The corrected voltage differences were then processed into electric potential by the signal processing approach described by Ikard and others (2018) and Ikard and others (2021a, 2021b), and the electric-potential data for each WaSP reach were combined into a continuous profile shown in Figure 4D.

The underlying physical mechanisms of streaming-current generation are generally well understood (Onsager, 1931a; Onsager, 1931b; Overbeek, 1952; Ishido and Mizutani, 1981; Sill, 1983; Ishido, 1989; Revil and others, 1999a; Revil and others, 1999b; Nyquist and Corry, 2002; Boléve and others, 2007; Sheffer and Oldenburg, 2007; Crespy and others, 2008; Haas and Revil, 2009; Cerepi and others, 2017; Revil and others, 2017). Streaming-current sources and sinks are attributed to GW flow through porous sediments and advection of counterions in a diffuse band of the electrical double layer that lines the pore-surfaces of the streambed sediments (Ikard and others, 2021b). During steady-state

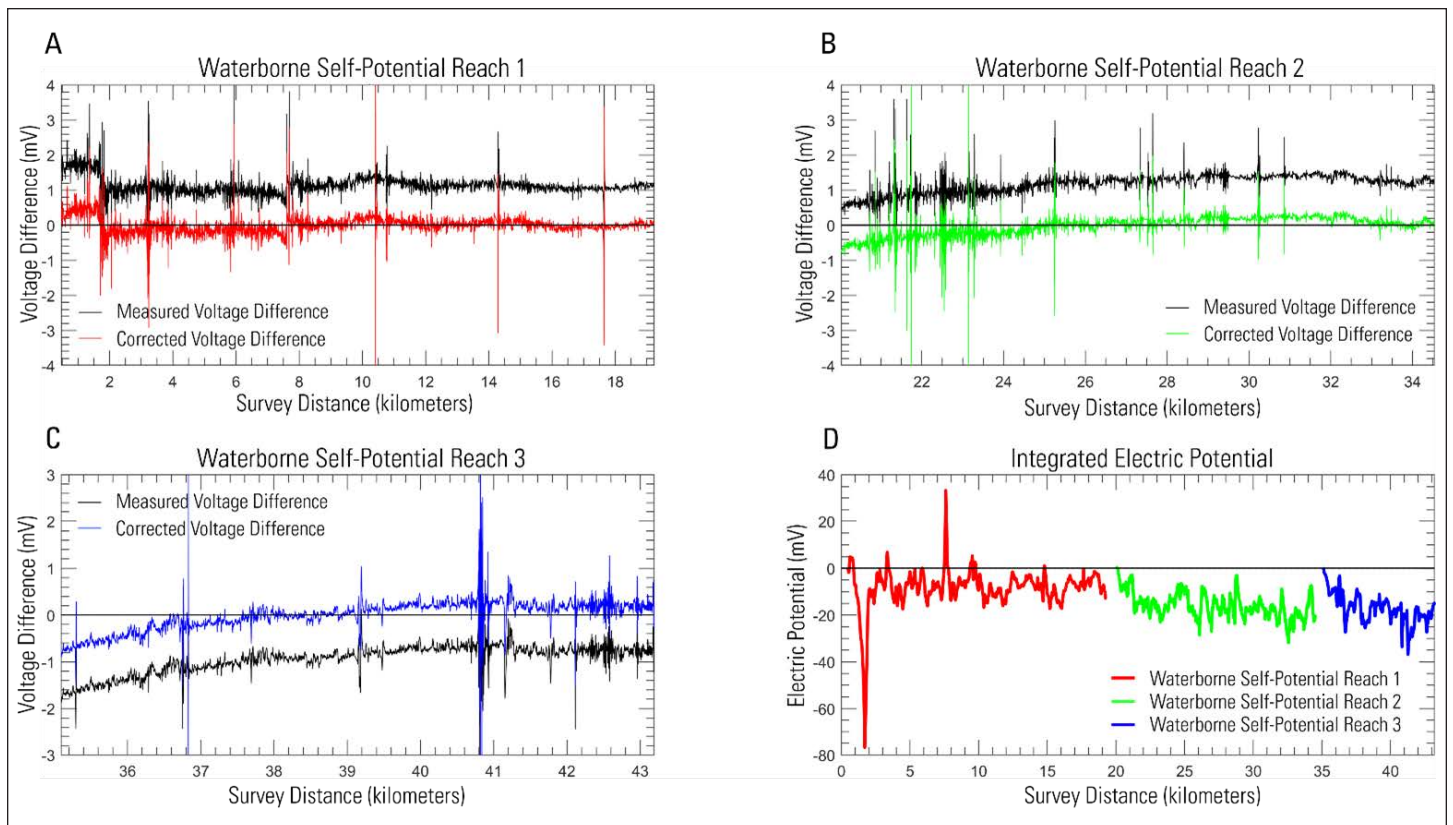


Figure 4. Graphs in panels A–C show the effects of applying terrain corrections to the measured voltage differences for (A) reach 1, (B) reach 2, and (C) reach 3. Graph in panel D shows the integrated electric potential profiles that were processed from the corrected voltages differences following the processing methods described by Ikard and others (2018) and Ikard and others (2021a, 2021b).

hydraulic conditions, GW flow is described by Equation 7 (Fetter, 2001; Anderson and others, 2015), where \mathbf{u} (m/s) is the Darcy velocity, $\nabla \cdot \mathbf{u}$ (1/s) is the divergence of Darcy velocity, and Q_s (1/s) represents a GW source (i.e. SW flow into the porous streambed sediments) when greater than zero and a GW sink (GW flow out of the streambed into the SW) when less than zero.

$$\nabla \cdot \mathbf{u} = \pm Q_s \quad (7)$$

The Darcy velocity is related to the hydraulic properties of the streambed sediments and the hydraulic-head distribution within the streambed and the aquifer by Equation 8, where K_s (m/s) is the saturated hydraulic conductivity, H (m) is the hydraulic head, and ∇H (m/m) is the hydraulic gradient. The hydraulic gradient is a vector whose direction is oriented from high to low hydraulic potential and controls the nature of SW-GW exchange between the stream and aquifer. Streams gain streamflow when the direction of the hydraulic gradient is from the aquifer toward the stream and lose streamflow when the direction of the hydraulic gradient is from the stream toward the aquifer (Anderson and others, 2015).

$$\mathbf{u} = -K_s \nabla H \quad (8)$$

On the streambed and submerged streambanks, GW flow into or out of the porous sediments generates streaming-current (\mathbf{j}_s ; A/m²) by advection of the excess volumetric charge density (\widehat{Q}_v) in the electric double layer coating the pore spaces in the streambed sediments. The intensities of the streaming currents generated by GW flow into or out of the streambed are described by the petrophysical relation in Equation 9 between streaming-current and Darcy velocity (Bolève and others, 2007), where \widehat{Q}_v in coulombs per cubic meter (C/m³) is expressed in terms of permeability (k ; m²) as shown in Equation 10 (Jardani and others, 2007; Jardani and others, 2008; Jardani and others, 2009; Cerepi and others, 2017).

$$\mathbf{j}_s = \widehat{Q}_v \mathbf{u} \quad (9)$$

$$\log_{10} \widehat{Q}_v = -9.2 - 0.82 * \log_{10} k \quad (10)$$

SW flow into the streambed (losing stream locations) creates streaming-current sinks and produces negative electric-potential anomalies on the streambed surface and saturated banks. Conversely, GW flow out of the streambed (gaining stream locations) creates streaming-current sources and produces positive streaming-potential anomalies on the streambed surface and saturated banks (Ernstson and Scherer, 1986; Ikard and others, 2021c). The streaming-potential field on the streambed and saturated banks attributed to the distribution and intensities of streaming-current sources and sinks at the streambed surface is described by the electrostatic equation shown in Equation 11, where ρ (ohm-m) is the resistivity of the streambed sediments.

$$\nabla \cdot (\rho^{-1} \nabla \varphi) = \nabla \cdot \mathbf{j}_s \quad (11)$$

The wetted perimeter of the stream channel defines a closed surface with respect to streaming-current generation (streaming currents are only generated by GW flow through porous geologic materials and therefore are not generated in SW); however, the electric-potential field is continuous from the porous sediments into the SW. Therefore, the electric-potential of the streambed and the submerged banks is electrically conducted from the streambed sediments, across the streambed surface, and into the SW where it can be measured by a WaSP survey if the signal-to-noise ratio is sufficiently large (Ikard and others, 2021b).

In addition to electric-potential data, SW temperature and conductivity data were collected during the WaSP survey in January 2022 (Ikard and others 2022). SW temperature and conductivity data were continuously logged at a period of 2 seconds per sample with an Onset HOB0 (Onset, Cape Cod, Massachusetts, <https://www.onsetcomp.com>) conductivity and temperature logger. Because heat travels through stationary and moving water, temperature measurements are well suited for water-exchange investigations (Constantz, 2008). Water-quality data such as conductivity measurements are valuable for assessing SW-GW exchanges and determining various sources of water based on differences in water-quality properties. For example, Baldys and Schalla (2016) discuss using the correlation of specific conductance and dissolved oxygen to evaluate water sources and streamflow gains and losses. Due to the complexity of heat transport related to diurnal and seasonal temperature variation temporally, it is important to evaluate diurnal patterns when assessing surface-water temperature changes regarding gaining and losing reaches of a stream (Ren and others, 2018). For this study, diurnal patterns were evaluated and only temperature gradients greater than the diurnal patterns were assessed as possible indicators of locations of GW-SW interaction. During the WaSP survey, the air temperature in the metropolitan area (as measured at Dallas Fort Worth International Airport) ranged

from 37–60°F, 27–50°F, and 37–51°F on January 25, 26, and 27, respectively (National Weather Service, 2023b). SW temperature and conductivity data with spatial and time-stamp information are available in Ikard and others (2022).

RESULTS AND DISCUSSION

The four discrete-measurement events were completed under a wide range of streamflow conditions; for example, streamflow at the farthest upstream site (streamgage 08053000) ranged from 207 to 1,610 ft³/s (Tables 3–7). Streamflow measurements indicate that the approximately 43-km-long (26.72 mile) surveyed reach of the Elm Fork was primarily gaining streamflow in the upper reaches and losing streamflow in the lower reaches during the study. Key locations of measured gains and losses are discussed in the “Conclusions” section of this report.

Streamflow Conditions of the Elm Fork Trinity River

During three of the four discrete measurement events, the average monthly rainfall totals were below the long-term average (1900 to 2022) for the metropolitan area at 0.4, 1.3, and 1.8 inches below average in October 2021, January 2022, and May 2022, respectively (National Weather Service, 2023c). Alternatively, during the May 2022 discrete measurement event, the monthly average was 8.3 inches above the long-term average at 10.7 in (National Weather Service, 2023c). Precipitation totals were also reviewed for seven days prior to each measurement event and the only measurable precipitation during those periods was for the October 2021 discrete measurement event, at 0.77 in on October 11, 2021 (National Weather Service, 2023b). Except for the October measurement event, the elevated (above base streamflow conditions) were due to releases from Lake Lewisville upstream of the survey reach (Figure 2).

Streamflow at streamgage 08053000 downstream from Lake Lewisville Dam was about 304, 207, 1,610, and 509 ft³/s during the October 2021, January 2022, May 2022, and August 2022 measurement events, respectively; farther downstream the streamflow at streamgage 08055500 near Carrollton Dam was about 220, 107, 1,490, and 170 ft³/s during the same discrete-measurement events (Tables 4–7, Figure 2). This appreciable decrease in streamflow is primarily the result of withdrawals at the Elm Fork WTP between the two streamgages. Withdrawal rates for a WTP for each discrete measurement event were not publicly available at the time of publication from Dallas Water Utilities. Withdrawal volumes were provided directly from Dallas Water Utilities in units of million gallons per day for this study. A constant withdrawal rate per day was then used to calculate average daily withdrawal rates for this study in ft³/s. Average daily withdrawal rates during the four discrete-measurement events were about

Table 3. Summary of discrete streamflow-measurement sites and water treatment plant (WTP) in the Elm Fork Trinity River between Lake Lewisville Dam and Frasier Dam. Discrete measurements made on the main stem are indicated in bold font and reaches are grouped by horizontal dashed lines. River distances were calculated from U.S. Geological Survey (USGS) streamgage 08053000 to the main-stem measurement location or confluence of the measured tributary.

| USGS streamgage number or site identifier | USGS streamgage or WTP | River distance from USGS streamgage 08053000 (km) | Latitude | Longitude | Description |
|---|--|---|----------------|---------------|------------------|
| 08053000 | Elm Fork Trinity River near Lewisville, Texas | 0.0 | -96.961 | 33.046 | Main Stem |
| 08053003 | Elm Fork Trinity River at Hebron Parkway near Lewisville, Texas | 6.5 | -96.951 | 33.013 | Main Stem |
| 08053009 | Indian Creek at FM 2281 Carrollton, Texas | 8.7 | -96.917 | 33.028 | Tributary |
| 08053018 | Dudley Branch at Rosemeade Parkway near Carrollton, Texas | 10.6 | -96.920 | 33.000 | Tributary |
| 08053020 | Elm Fork Trinity River at IH-35E near Lewisville, Texas | 11.3 | -96.949 | 32.993 | Main Stem |
| 08053027 | Timber Creek at Waters Ridge Drive near Lewisville, Texas | 11.9 | -96.974 | 33.010 | Tributary |
| 08053040 | Furneaux Creek at Old Denton Road near Carrollton, Texas | 13.6 | -96.910 | 32.990 | Tributary |
| WTP | Water Treatment Plant Withdrawal | 15.1 | -- | -- | Withdrawal |
| 08055350 | Denton Creek at N. MacArthur Boulevard near Coppell, Texas | 15.8 | -96.974 | 32.989 | Tributary |
| 08055500 | Elm Fork Trinity River near Carrollton, Texas | 16.4 | -96.945 | 32.966 | Main Stem |
| 08053090 | Hutton Branch at N. Denton Drive at Carrollton, Texas | 19.3 | -96.907 | 32.957 | Tributary |
| 08055515 | Grapevine Creek at N. MacArthur Boulevard near Irving, Texas | 20.2 | -96.958 | 32.950 | Tributary |
| 08055516 | Cooks Branch at Hutton Drive near Dallas, Texas | 22.8 | -96.914 | 32.925 | Tributary |
| 08055518 | Farmers Branch at N. Stemmons Freeway near Dallas, Texas | 26.3 | -96.900 | 32.916 | Tributary |
| 08055519 | Farmers Branch Tributary at IH 635 Service Road near Dallas, Texas | 26.3 | -96.906 | 32.909 | Tributary |
| 08055538 | Hackberry Creek at Love Drive at Irving, Texas | 28.7 | -96.954 | 32.889 | Tributary |
| 08055555 | Cottonwood Branch at John Carpenter Freeway near Irving, Texas | 28.7 | -96.946 | 32.877 | Tributary |
| 08055560 | Elm Fork Trinity River at Spur 348, Irving, Texas | 30.1 | -96.931 | 32.874 | Main Stem |
| 08055600 | Joes Creek at Dallas, Texas | 37.7 | -96.884 | 32.859 | Tributary |
| 08055620 | Elm Fork Trinity River at Spur 482 near Irving, Texas | 38.2 | -96.893 | 32.848 | Main Stem |

[--; not available, USGS; U.S. Geological Survey, km; kilometers, WTP; water treatment plant]

221 ft³/s on October 12, 2021, 182 ft³/s on January 25, 2022, 310 ft³/s on May 17, 2022, and 363 ft³/s on August 9, 2022 (Tables 4–7). Additional permitted Elm Fork withdrawal volumes were also provided by DWU but were negligible relative to streamflow during the four discrete-measurement events. After accounting for WTP withdrawals in the reach between streamgages 08053000 and 08055500, gains were measured in three of the four discrete-measurement events (Figures 5 and 6); however, the estimated gain in May 2022 was less than the combined measurement uncertainty. The slight loss of approx-

imately 8 ft³/s in that reach was measured during the August 2022 measurement event but was also less than the combined measurement uncertainty (Table 7). Streamflow in the lower reach of the study area showed both gains and losses during various streamflow and seasonal climatic conditions relative to the upstream streamgage and was time-lagged relative to minimums and peaks in streamflow upstream at streamgage 08055500. Downstream from streamgage 08055500 streamflow losses of about 13.6, 95.4, and 9.6 ft³/s were observed during the January, May, and August 2022 discrete-measure-

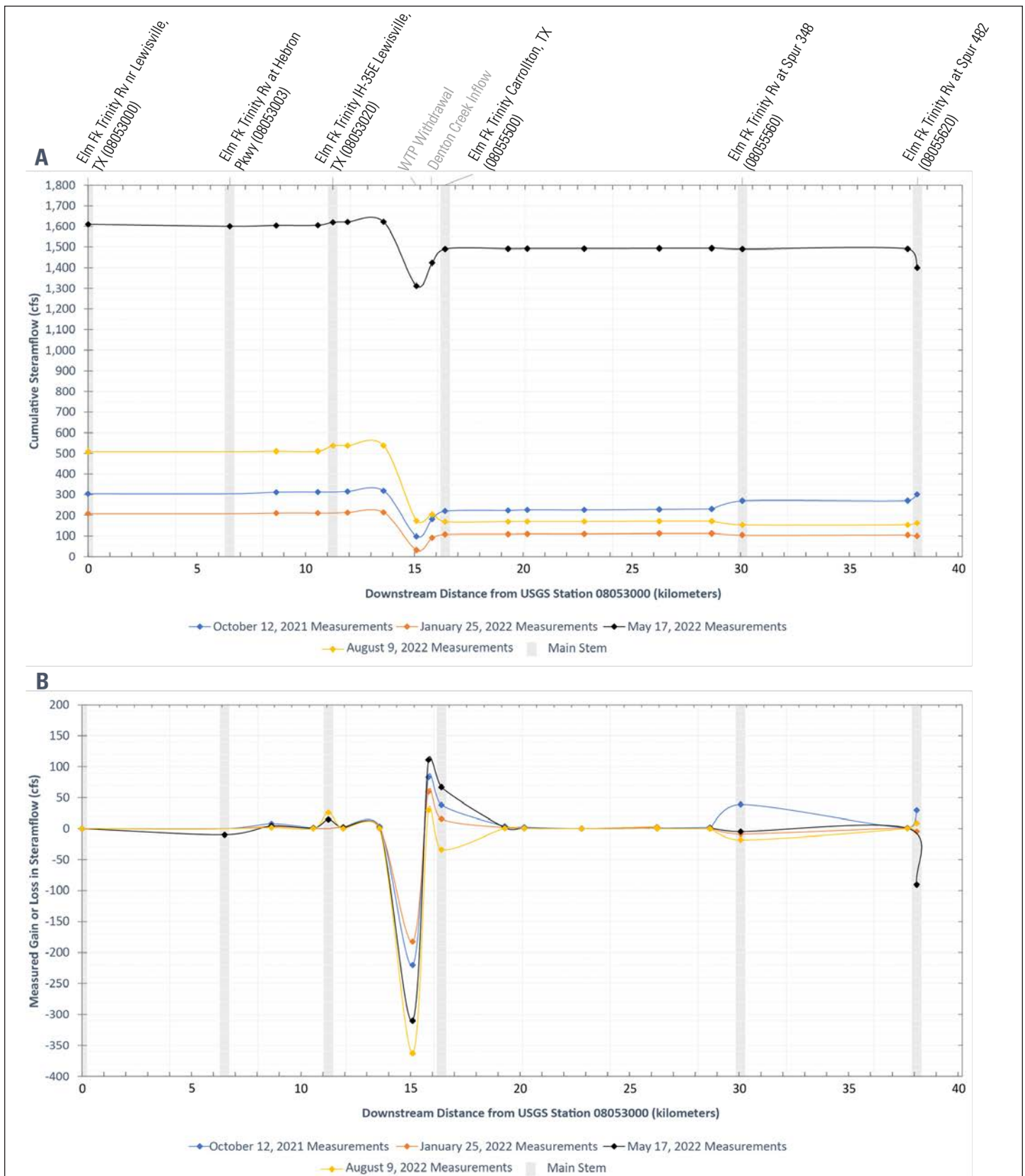


Figure 5. Graph showing cumulative streamflow gaining and losing reaches in cubic feet per second (ft^3/s) during the four discrete-measurement events in October 2021, and January, May, and August 2022 along the Elm Fork Trinity River between Lake Lewisville Dam and Frasier Dam. Shaded tan columns show locations of main-stem Elm Fork Trinity River discrete measurements. Between main-stem measurements, streamflow gains are highlighted in blue and losses in red when the gain or loss exceeds the total measurement uncertainty and gray when less than the uncertainty.

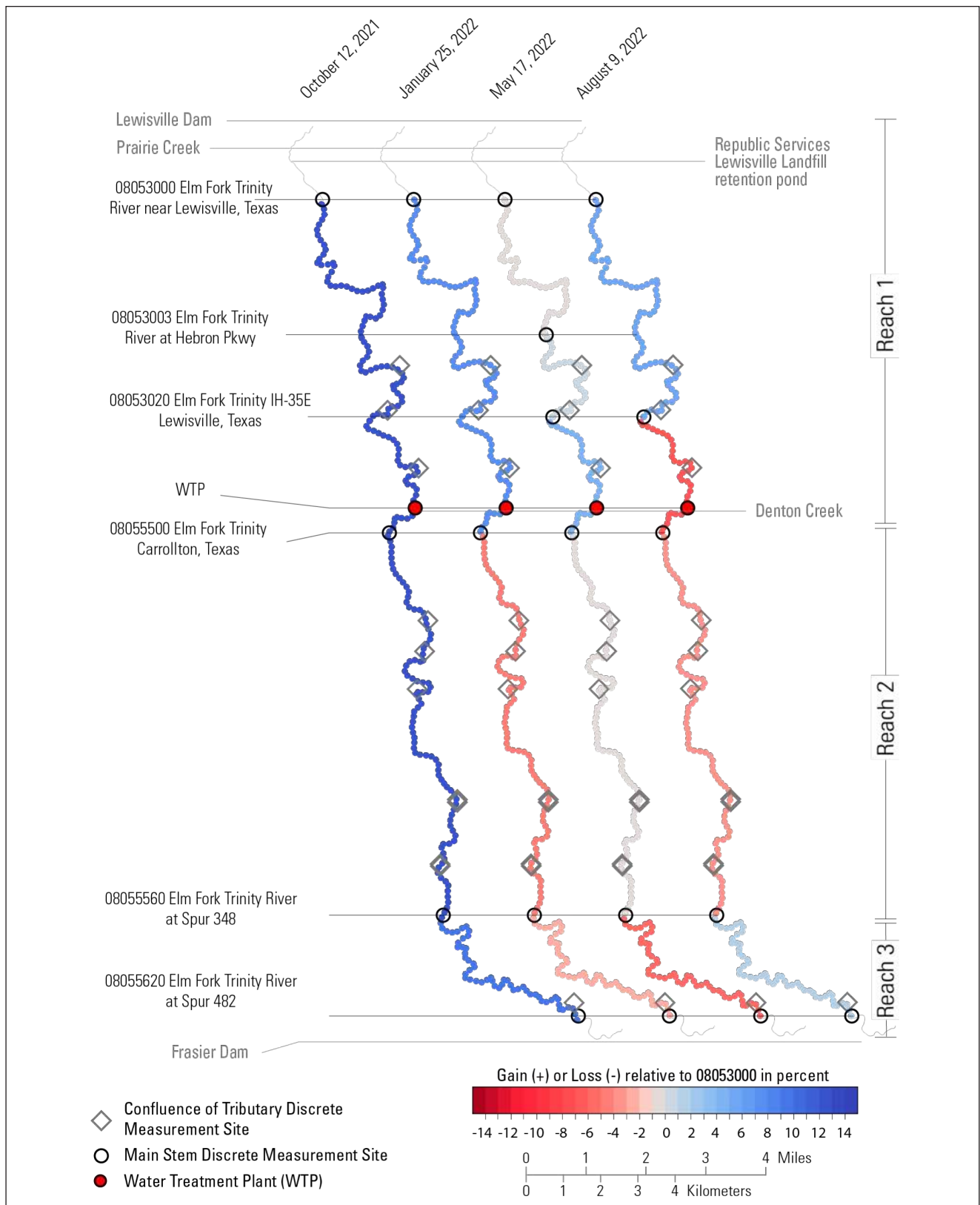


Figure 6. Graph showing gains and losses in percent of streamflow relative to the streamflow at U.S. Geological Survey streamgage 08053000 during the four discrete-measurement events in October 2021, and January, May, and August 2022 along the Elm Fork Trinity River between Lake Lewisville Dam and Frasier Dam.

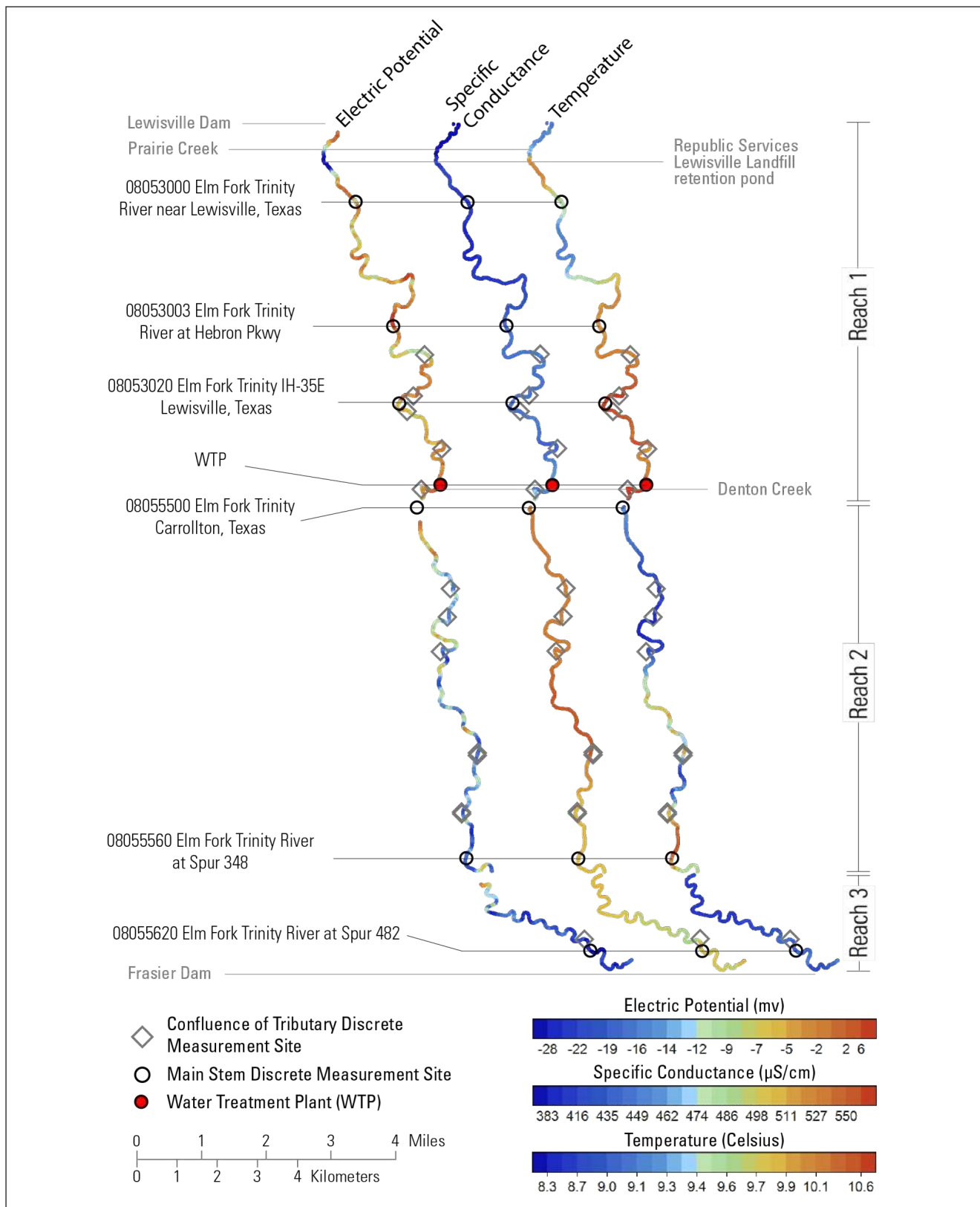


Figure 7. Map surface-water electric potential in millivolts (mV), specific conductance in microsiemens per centimeter at 25 degrees Celsius (µS/cm), and temperature in degrees Celsius (°C) from the waterborne self-potential (WaSP) survey in January 2022 along the Elm Fork Trinity River between Lake Lewisville Dam and Frasier Dam.

Table 4. Summary of discrete streamflow measurements and water treatment plant (WTP) withdrawals in the Elm Fork Trinity River between Lake Lewisville Dam and Frasier Dam on October 12, 2021. Discrete measurements made on the main stem are indicated in bold font and reaches are grouped by horizontal dashed lines. Between main-stem measurements, streamflow gains are highlighted in blue when the gain exceeds the total measurement uncertainty. Streamflow data from U.S. Geological Survey (2023).

| USGS streamgage number or site identifier | Measured streamflow (ft ³ /s) | Measurement uncertainty (ft ³ /s) | Cumulative streamflow in the main stem (ft ³ /s) | Total measurement uncertainty for a given reach (ft ³ /s) | Streamflow gain (+) or loss (-) per reach (ft ³ /s) | Gain or loss relative to USGS streamgage 08053000 (%) |
|---|--|--|---|--|--|---|
| 08053000 | 304 | 6.08 | 304 | | | |
| 08053009 | 7.86 | 0.157 | 312 | | | |
| 08053018 | 0.89 | 0.089 | 313 | | | |
| 08053027 | 2.71 | 0.054 | 315 | | | |
| 08053040 | 3.39 | 0.170 | 319 | | | |
| WTP | -221 | | 98.3 | | | |
| 08055350 | 83.3 | 4.17 | 182 | 15.1 | +38.4 | 12.6 |
| 08055500 | 220 | 4.40 | 220 | | | |
| 08053090 | 3.79 | 0.379 | 224 | | | |
| 08055515 | 2.27 | 0.114 | 226 | | | |
| 08055516 | 0.00 | 0.000 | 226 | | | |
| 08055518 | 2.04 | 0.204 | 228 | | | |
| 08055519 | 0.38 | 0.038 | 228 | | | |
| 08055538 | 1.96 | 0.196 | 230 | | | |
| 08055555 | 0.47 | 0.047 | 231 | 18.9 | +39.1 | 12.9 |
| 08055560 | 270 | 13.5 | 270 | | | |
| 08055600 | 1.06 | 0.106 | 271 | 28.7 | +29.9 | 9.8 |
| 08055620 | 301 | 15.1 | 301 | | | |
| <i>Gain or Loss over full reach</i> | | | | | +107.4 | 35.3 |

ment events, respectively (Tables 4–7). A gain in streamflow of about 69 ft³/s was observed during the October 2021 discrete-measurement event. A more in-depth evaluation of these gaining and losing reaches is provided in the “Conclusions” section of this report.

Waterborne Self-potential, Surface-Water Temperature, and Surface-Water Conductivity

The largest electric-potential anomaly occurs along WaSP reach 1 (approximately 1 mile downstream from the start of the WaSP reach 1; Figure 7). Electric-potential results processed from the measured voltage data indicate that streamflow losses may occur at a focused location in the northern part of WaSP reach 1 and losses and gains may be more distributed along WaSP reaches 2–3. A notable change in both the measured voltage differences and in the processed electric potential occurs near the inflow of Prairie Creek and adjacent Repub-

lic Services Lewisville Landfill retention pond. This effect is shown in the WaSP reach 1 data in Figure 4D and in the electric potential in Figure 7 and further discussed in the “Conclusions” section of this report.

The electric-potential profile data support the qualitative interpretation that the individual WaSP reaches generally represented distributed losing conditions. In general, the electric-potential profile data along the full WaSP reach depict observable decreases at the downstream ends of the reaches and relative increases in electric potential at the upstream ends of the reaches, which reflects the localized reductions in hydraulic gradient attributed to low-head dams positioned at these locations that produce localized losing conditions on the upstream sides and localized gaining conditions on the downstream sides of the low-head dams. The electric-potential data further indicate that some short, interspersed stream reaches may be characterized by discrete gains or losses of varying magnitudes, and these discrete gains or losses appear to occur over spatial scales

Table 5. Summary of discrete streamflow measurements and water treatment plant (WTP) withdrawals in the Elm Fork Trinity River between Lake Lewisville Dam and Frasier Dam on January 25, 2022, during the waterborne self-potential logging survey. Discrete measurements made on the main stem are indicated in bold font and reaches are grouped by horizontal dashed lines. Between main-stem measurements, streamflow gains are highlighted in blue and losses in red when the gain or loss exceeds the total measurement uncertainty. Streamflow data from U.S. Geological Survey (2023).

| USGS streamgage number or site identifier | Measured streamflow (ft ³ /s) | Measurement uncertainty (ft ³ /s) | Cumulative streamflow in the main stem (ft ³ /s) | Total measurement uncertainty for a given reach (ft ³ /s) | Streamflow gain (+) or loss (-) per reach (ft ³ /s) | Gain or loss relative to USGS streamgage 08053000 (%) |
|---|--|--|---|--|--|---|
| 08053000 | 207 | 4.14 | 207 | | | |
| 08053009 | 3.33 | 0.33 | 210 | | | |
| 08053018 | 0.18 | 0.02 | 211 | | | |
| 08053027 | 2.22 | 0.04 | 213 | | | |
| 08053040 | 1.02 | 0.10 | 214 | | | |
| WTP | -182 | | 31.4 | | | |
| 08055350 | 59.9 | 1.20 | 91.3 | 7.98 | +15.7 | 7.6 |
| 08055500 | 107 | 2.14 | 107 | | | |
| 08053090 | 1.54 | 0.15 | 109 | | | |
| 08055515 | 0.98 | 0.02 | 110 | | | |
| 08055516 | 0.01 | 0.00 | 110 | | | |
| 08055518 | 2.69 | 0.27 | 112 | | | |
| 08055519 | 0.13 | 0.01 | 112 | | | |
| 08055538 | 0.36 | 0.01 | 113 | | | |
| 08055555 | 0.00 | 0.00 | 113 | 4.68 | -8.71 | -4.2 |
| 08055560 | 104 | 2.08 | 104 | | | |
| 08055600 | 0.93 | 0.09 | 105 | 4.17 | -4.93 | -2.4 |
| 08055620 | 301 | 15.1 | 301 | | | |
| <i>Gain or Loss over full reach</i> | | | | | +2.04 | 1.0 |

ranging from a few hundred meters to about 2–2.5 km along reach 1. For example, polarity reversals from negative to positive electric-potential occur at locations along survey reach 1 between survey profile distances of about 0.6–0.9, 3–3.5, 7.5–8, and 9.4–9.8 km downstream from the survey starting point. These locations correspond to positive electric-potential anomalies characterized by magnitudes of about 5, 7, 33, and 6 mV, respectively. Relatively discrete losses are indicated along reach 1 between survey distances of about 1 km and 3.5 km downstream from the survey start point. The conspicuous reduction in electric-potential over this reach length corresponds to a negative electric-potential anomaly with a magnitude that decreases to less than -70 mV adjacent to a retention pond on the west flood-plain of the Elm Fork. The electric-potential profiles along WaSP reaches 2 and 3 each displayed predominantly negative electric-potential values and negative slopes in the profile data whereby increasing downstream distance corresponds to decreasing electric potential in the stream. The neg-

ative slope of the electric-potential data increases along WaSP reach 2 relative to the slope of the profile data along WaSP reach 1, and increases again along WaSP reach 3 relative to the electric-potential profile data along WaSP reach 2. Spatial patterns in the electric-potential data along WaSP reaches 2 and 3 (relative increases and decreases in the electric-potential data along the profile) appear to vary over a kilometeric scale, predominantly between about 1–3 km.

Specific conductance data in microsiemens per centimeter at 25 degrees Celsius ($\mu\text{S}/\text{cm}$) were calculated from the SW temperature in degrees Celsius ($^{\circ}\text{C}$) and SW conductivity data ($\mu\text{S}/\text{cm}$) (U.S. Geological Survey, 2019) (Figure 8C). A general pattern in the relation between SW temperature and specific conductance was observed for each WaSP reach, and perhaps multiple different patterns along each individual WaSP reach (Figure 8D). Higher temperatures and lower specific conductance values were recorded in WaSP reach 1 compared to WaSP reaches 2–3.

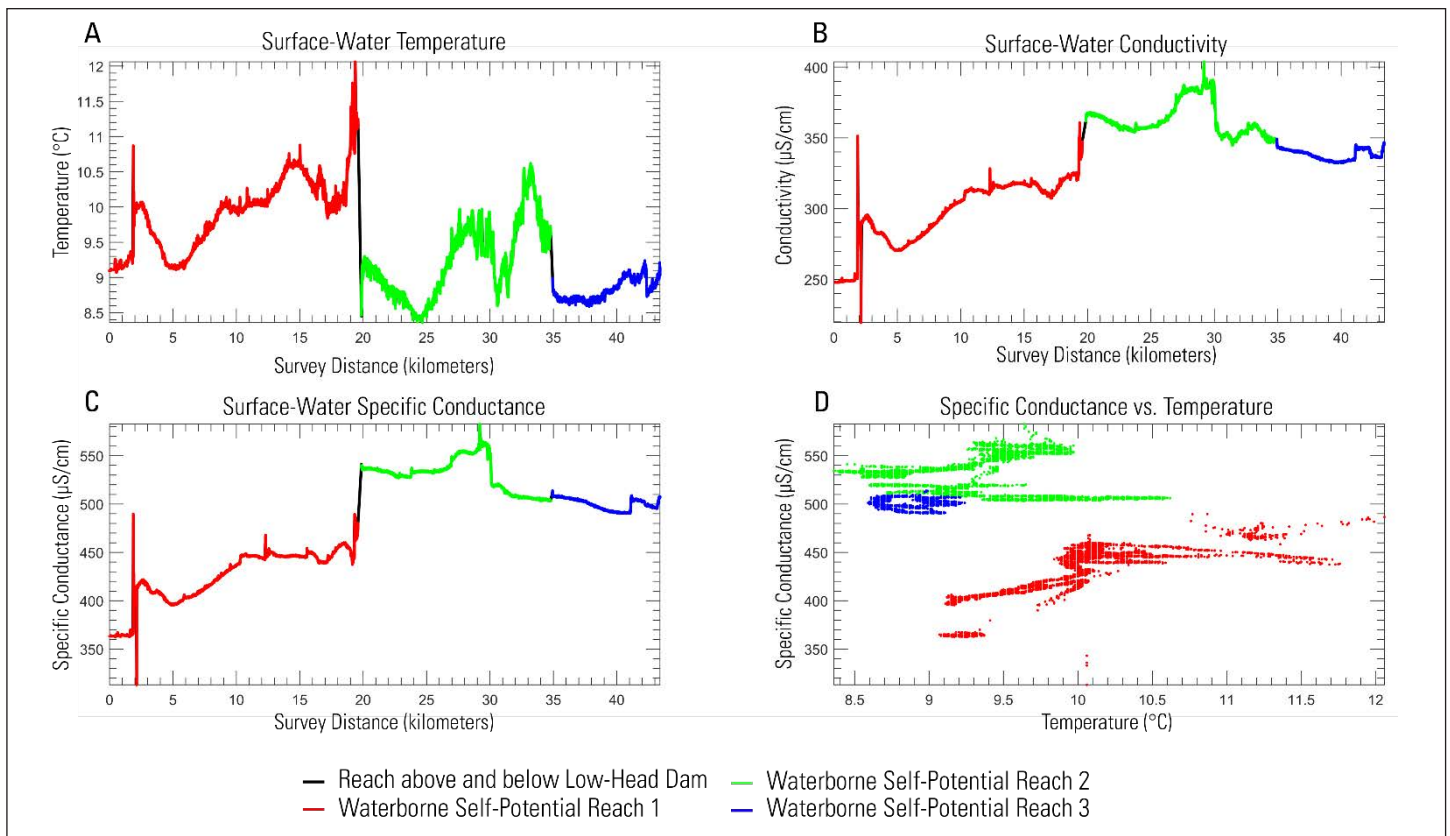


Figure 8. (A) Surface-water temperature in degrees Celsius (°C) and (B) conductivity in microsiemens per centimeter (µS/cm) data measured along each waterborne self-potential (WaSP) survey reach of the Elm Fork Trinity River between Lake Lewisville Dam and Frasier Dam. (C) Calculated surface-water specific conductance in µS/cm at 25 degrees Celsius from the measured surface-water temperature and conductivity along each WaSP survey reach. (D) Scatterplot of temperature and specific conductance for each WaSP reach. Reaches are depicted in black for areas directly upstream or downstream of low-head dams, where surface-water temperature and conductivity were not collected (Figure 1).

CONCLUSIONS

Overall, the measurements in the Elm Fork reach between Lake Lewisville Dam and Frasier Dam indicated both gains and losses in streamflow during this study over a wide range of streamflow conditions (207 to 1,610 ft³/s at USGS stream-gage 08053000 Elm Fork Trinity River near Lewisville, Texas (stream-gage 08053000) after accounting for inflows from measured tributaries and withdrawals at a WTP. Average WTP withdrawal rates ranged from a minimum of about 182 ft³/s on January 25, 2022, to a maximum of about 363 ft³/s on August 9, 2022, during discrete-measurement events. The only discrete measurement event with a calculated gain over the full reach greater than the measurement uncertainty, was during the October 2021 measurement event that followed 0.77 in of precipitation the day prior. The largest loss for the full reach was observed during the August measurement event, where approximately 3 percent of the streamflow from stream-gage 0853000 was estimated to be lost but was less than the measurement uncertainty. Accounting for measured tributary inflows to the

Elm Fork in this reach, streamflow gains and losses were primarily observed in three locations: between Lake Lewisville Dam and stream-gage 08053000, between USGS stream-gages 08053020 Elm Fork Trinity River at IH-35E near Lewisville, Texas and 08055500 Elm Fork Trinity River near Carrollton, Texas, and between USGS stream-gages 08055560 Elm Fork Trinity River at Spur 348, Irving, Texas and 08055620 Elm Fork Trinity River at Spur 482 near Irving, Texas.

SW temperature and specific-conductance profile data show some spatial changes collocated with electric-potential anomalies along WaSP reach 1, and otherwise show spatial patterns that vary on a predominantly kilometeric scale. GW temperatures generally are more stable than SW temperatures and are therefore well suited for identifying SW-GW interactions (Winter and others, 1999). The negative electric-potential anomaly observed along WaSP reach 1 at survey distance of 1 to 3 km is collocated with a notable increase in SW temperature and SW specific-conductance data that appears initially as a discrete increase over a short segment of the profile followed by a more gradual decrease to about 5 km downstream from

Table 6. Summary of discrete streamflow measurements and water treatment plant (WTP) withdrawals in the Elm Fork Trinity River between Lake Lewisville Dam and Frasier Dam on May 17, 2022. Discrete measurements made on the main stem are indicated in bold font and reaches are grouped by horizontal dashed lines. Between main-stem measurements, streamflow losses are highlighted in red when the loss exceeds the total measurement uncertainty. No streamflow gains exceeded the total measurement uncertainty. Streamflow data from U.S. Geological Survey (2023).

| USGS streamgage number or site identifier | Measured streamflow (ft ³ /s) | Measurement uncertainty (ft ³ /s) | Cumulative streamflow in the main stem (ft ³ /s) | Reach uncertainty (ft ³ /s) | Streamflow gain (+) or loss (-) per reach (ft ³ /s) | Gain or loss relative to USGS streamgage 08053000 (%) |
|---|--|--|---|--|--|---|
| 08053000 | 1,610 | 32.2 | 1,610 | 64.2 | -10.0 | -0.6 |
| 08053003 | 1,600 | 32.0 | 1,600 | | | |
| 08053009 | 4.27 | 0.43 | 1,604 | | | |
| 08053018 | 1.02 | 0.10 | 1,605 | 64.9 | +14.7 | 0.9 |
| 08053020 | 1,620 | 32.4 | 1,620 | | | |
| 08053027 | 1.70 | 0.17 | 1,622 | | | |
| 08053040 | 0.48 | 0.05 | 1,622 | | | |
| WTP | -310 | | 1,312 | | | |
| 08055350 | 111 | 11.10 | 1,423 | 118 | +67.1 | 4.2 |
| 08055500 | 1,490 | 74.5 | 1,490 | | | |
| 08053090 | 1.55 | 0.08 | 1,492 | | | |
| 08055515 | 0.68 | 0.01 | 1,492 | | | |
| 08055516 | 0.00 | 0.00 | 1,492 | | | |
| 08055518 | 0.89 | 0.09 | 1,493 | | | |
| 08055519 | 0.54 | 0.05 | 1,494 | | | |
| 08055538 | 0.07 | 0.01 | 1,494 | 105 | -4.8 | -0.3 |
| 08055560 | 1,490 | 29.8 | 1,490 | | | |
| 08055600 | 0.62 | 0.06 | 1,491 | 57.9 | -90.6 | -5.6 |
| 08055620 | 1,400 | 28.0 | 1,400 | | | |
| <i>Gain or Loss over full reach</i> | | | | | -23.6 | -1.5 |

the start point, and then a general increase over another 9–10 km in a downstream direction. In general, the SW temperature profile showed the largest gradients at locations of mixing SW sources. Along WaSP reach 1 the SW temperature profile showed downstream warming SW conditions throughout the collection period with anomalies larger than the diurnal pattern near the confluence of Prairie Creek and the Republic Services Lewisville Landfill retention pond, a WTP, and inflow from Timber Creek. Specific-conductance values in WaSP reach 1 were relatively stable to the confluence of Denton Creek, where higher values were measured downstream. The SW temperature profile data along reach 2 showed two primary deflections, with cooler SW below Farmer Branch tributary and warmer SW below the confluence of Hackberry Creek and Cottonwood Branch. SW temperatures in the WaSP reach 3 were relatively constant. Relative to WaSP reach 1, elevated specific-conductance values were measured in WaSP reach 2. Spe-

cific conductance along reach 2 slightly decreased below the confluence of Farmers Branch and remained relatively constant downstream.

Whereas the uppermost streamflow measurement was made at the Elm Fork River near Lewisville streamgage 08053000, the WaSP survey completed in January 2022 started below Lake Lewisville Dam. The large negative spontaneous potential (SP) anomaly and shift in SW temperature observed just downstream from Lake Lewisville Dam, is spatially aligned with the outflow to Prairie Creek and a retention pond associated with a waste-disposal site (Figure 1). Two possible hypotheses for these results are: (1) a hydraulic gradient exists from the Elm Fork to the retention pond causing the Elm Fork to lose water to the retention pond, or (2) a subsurface redox plume associated with the presence of the waste-disposal site is producing the negative SP anomaly. The first hypothesis has been shown to be capable of producing a negative SP anomaly by

Table 7. Summary of discrete streamflow measurements and water treatment plant (WTP) withdrawals in the Elm Fork Trinity River between Lake Lewisville Dam and Frasier Dam on August 9, 2022. Discrete measurements made on the main stem are indicated in bold font and reaches are grouped by horizontal dashed lines. Between main-stem measurements, streamflow losses are highlighted in red when the loss exceeds the total measurement uncertainty. No streamflow gains exceeded the total measurement uncertainty. Streamflow data from U.S. Geological Survey (2023).

| USGS streamgage number or site identifier | Measured streamflow (ft ³ /s) | Measurement uncertainty (ft ³ /s) | Cumulative streamflow in the main stem (ft ³ /s) | Reach uncertainty (ft ³ /s) | Streamflow gain (+) or loss (-) per reach (ft ³ /s) | Gain or loss relative to USGS streamgage 08053000 (%) |
|---|--|--|---|--|--|---|
| 08053000 | 509 | 25.5 | 509 | | | |
| 08053009 | 1.72 | 0.03 | 511 | | | |
| 08053018 | 0.16 | 0.02 | 511 | 36.2 | +26.1 | 5.1 |
| 08053020 | 537 | 10.7 | 537 | | | |
| 08053027 | 0.00 | 0.00 | 537 | | | |
| 08053040 | 0.16 | 0.02 | 537 | | | |
| WTP | -363 | 0.00 | 174 | | | |
| 08055350 | 29.8 | 0.60 | 204 | 14.8 | -34.1 | -6.7 |
| 08055500 | 170 | 3.40 | 170 | | | |
| 08053090 | 0.47 | 0.05 | 170 | | | |
| 08055515 | 0.54 | 0.05 | 171 | | | |
| 08055516 | 0 | 0.00 | 171 | | | |
| 08055518 | 1.13 | 0.11 | 172 | | | |
| 08055519 | 0.05 | 0.01 | 172 | | | |
| 08055538 | 0.2 | 0.02 | 172 | | | |
| 08055555 | 0.00 | 0.00 | 172 | 6.72 | -18.4 | -3.6 |
| 08055560 | 154 | 3.08 | 154 | | | |
| 08055600 | 0.19 | 0.02 | 154 | 11.2 | +8.81 | 1.7 |
| 08055620 | 163 | 8.15 | 163 | | | |
| <i>Gain or Loss over full reach</i> | | | | | -17.6 | -3.4 |

Ikard and others (2018), Valois and others (2017), Ikard and others (2021a), and Ikard and others (2021b), whereas the second hypothesis has been shown to be capable of producing a negative SP anomaly by Hämmann and others (1997), Timm and Möller (2001), Nyquist and Corry (2002), and Naudet and others (2003).

Between streamgage 08053000 and streamgage 08055500, the largest inflows and withdrawals occur. The only major source of withdrawals on this reach of the Elm Fork was for a WTP; these withdrawals were responsible of the largest changes in streamflow during the study period. During each discrete-measurement event, the inflow from Denton Creek was the largest inflow from any tributary. Inflow from Denton Creek during the discrete-measurement events was about 83 ft³/s on October 12, 2021, 60 ft³/s on January 25, 2022, 111 ft³/s on May 17, 2022, and 30 ft³/s on August 9, 2022. After accounting for the WTP withdrawals and inflows from measured tributaries, streamflow gains were measured during three of the four discrete-measurement events; however, the streamflow gain in May 2022 was less than the measurement uncertainty for that reach. These gains in October 2021 and January 2022 ranged from about 16 ft³/s to 38 ft³/s, respectively. During the final discrete-measurement event on August 9, 2022, a loss of about 8 ft³/s was measured between streamgages 08053000 and 08055500 but was within the uncertainty of the measurements for that reach. This potential loss is likely the result of measurement uncertainty or drier and hotter conditions during the August 2022 measurement event relative to the others. The downstream reach between streamgages 08055500 and 08055560 also had the only loss of more than 10 ft³/s during the August 2022 discrete-measurement event and was nearly three times larger than the measurement uncertainty, this loss is likely a result of extremely dry and hot conditions that prevailed during this measurement event.

Both gains and losses were observed in the reach between the Elm Fork Trinity River at Spur 348 (08055560) and Elm Fork Trinity River at Spur 482 (08055620) streamgages, depending on streamflow conditions. During the discrete measurements in January and August 2022, streamflow was relatively stable with a loss of about 5 ft³/s and a gain of about 9 ft³/s, respectively but the gain in August 2022 was within the measurement uncertainty. A 0.77 precipitation event was recorded on October 11, 2021 and corresponded to a peak computed streamflow of 993 ft³/s obtained from the continuous streamgage at Spur

348 (08055560) that showed elevated streamflow, compared to the conditions found during the discrete streamflow measurement of 270 ft³/s on October 12, 2021. A gain of about 30 ft³/s was observed during the October 2021 discrete-measurement event in this reach and is likely a result of runoff from the precipitation event and drainage of SW from low lying areas adjacent to the Elm Fork that were inundated by streamflow the day prior. The upstream reach between streamgages 08055500 and 08055560 also had the only gaining discrete-measurement event during October 2021 likely due to the same conditions. Conversely, during the highest streamflow measured in this study (about 1,610 ft³/s at 08053000), a loss of about 91 ft³/s was measured in this reach during the August 2022 discrete event and is likely due to increases in SW storage of low-lying areas.

Due to the complex nature of gaining and losing conditions over the relatively long reach assessed during this study, there are likely still additional studies needed to fully understand these conditions under all hydrologic and seasonal climatic conditions. Additional rounds of discrete measurements, coupled with continuous streamflow information, would build on results of this study, and overall improve the spatial and temporal understanding of gaining and losing conditions in the reach. The results from this study, completed over a wide range of streamflow, and seasonal conditions, provide Dallas Water Utilities and other water resource managers vital synoptic results to inform their water management strategies. This information will enable water resource managers information to evaluate gaining and losing impacts under similar conditions that were observed during this study to help maximize water resources.

ACKNOWLEDGMENTS

The authors thank Denis Qualls and Semu Moges with the City of Dallas for their support in the development of this study, assistance in obtaining access to sites, and WTP withdrawal information throughout the study duration. The authors also thank the U.S. Geological Survey, Oklahoma-Texas Water Science Center, North Texas Data Section for their assistance in discrete streamflow measurements and sharing their expertise of the hydrology of the study area. Any use of trade, firm, or product names is for descriptive purposes only and does not imply endorsement by the U.S. Government.

REFERENCES

- Allen, P.M., and Flanigan, W.D., 1986, *Geology of Dallas, Texas, United States of America: Bulletin of the Association of Engineering Geologists*, v. XXIII, no. 4., p. 363–418, accessed May 17, 2023, at <https://doi.org/10.2113/gseegeosci.xxiii.4.359>.
- Anderson, M.P., Woessner, W.W., and Hunt, R.J., 2015, *Applied groundwater modeling (2d ed.): Simulation of flow and advective transport*, Academic Press, Inc., London, 564 p.
- Baldys, Stanley, III, and Schalla, F.E., 2016, Base flow (1966–2009) and streamflow gain and loss (2010) of the Brazos River from the New Mexico–Texas State line to Waco, Texas (ver. 1.1, June 2016): U.S. Geological Survey Scientific Investigations Report 2011–5224, 53 p., accessed May 17, 2023, at <http://dx.doi.org/10.3133/sir20115224>.
- Barde-Cabusson, S., Finizola, A., and Grobde, N., 2021, A practical approach for self-potential data acquisition, processing, and visualization: *Interpretation*, v. 9, no. 1, p. T123–T143, Accessed May 17, 2023, at <https://doi.org/10.1190/INT-2020-0012.1>.
- Blakely, R.J., 1996, *Potential theory in gravity and magnetic applications*: New York, N.Y., Cambridge University Press, 441p.
- Bolève, A., Revil, A., Janod, F., Mattiuzzo, J.L., and Jardani, A., 2007, Forward modeling and validation of a new formulation to compute self-potential signals associated with ground water flow: *Hydrology and Earth Systems Sciences*, v. 11, no. 5, p. 1661–1671, accessed May 17, 2023, at <https://doi.org/10.5194/hess-11-1661-2007>.
- Braun, C.L., and Grzyb, S.D., 2015, Streamflow gains and losses in the Colorado River in northwestern Burnet and southeastern San Saba Counties, Texas, 2012–14: U.S. Geological Survey Scientific Investigations Report 2015–5098, 32 p., accessed May 17, 2023, at <http://doi.org/10.3133/sir20155098>.
- Cerepi, A., Cherubini, A., Garcia, B., Deschamps, H., and Revil, A., 2017, Streaming potential coupling coefficient in unsaturated carbonate rocks: *Geophysical Journal International*, v. 210, no. 1, p. 291–302, accessed May 17, 2023 at <https://doi.org/10.1093/gji/ggx162>.
- Coffman, D.K., Malstaff, G., and Heitmuller, F.T., 2011, Characterization of geomorphic units in the alluvial valleys and channels of Gulf Coastal Plain rivers in Texas, with examples from the Brazos, Sabine, and Trinity Rivers, 2010: U.S. Geological Survey Scientific Investigations Report 2011–5067, 42 p., May 17, 2023, at <https://doi.org/10.3133/sir20115067>.
- Constantz, J., 2008, Heat as a tracer to determine streambed water exchanges: *American Geophysical Union*, v. 44, no. 4, accessed May 17, 2023, at <https://doi.org/10.1029/2008WR006996>.
- Crespy, A., Revil, A., Linde, N., Byrdina, S., Jardani, A., Bolève, A. and Henry, P., 2008, Detection and localization of hydromechanical disturbances in a sandbox using the self-potential method: *Journal of Geophysical Research*, v. 113, no. B1, p. 1–23, accessed May 17, 2023, at <https://doi.org/10.1029/2007JB005042>.
- Dallas Water Utilities, 2019, City of Dallas—2019 Water Conservation Plan, accessed May 17, 2023, at https://savedallaswater.com/wp-content/uploads/2019/05/2019-Water-Conservation-Plan_Submitted.pdf.
- Ernstson, K., and Scherer, H.U., 1986, Self-potential variations with time and their relation to hydrogeologic and meteorological parameters: *Geophysics*, v. 51, no. 10, p.1967–1977, accessed May 17, 2023, at <https://doi.org/10.1190/1.1442052>.
- Fetter, C.W., 2001, *Applied Hydrogeology (4th ed.)*, Prentice-Hall, Inc., New Jersey, 598 p.
- Fuchs, E.H., King, J.P., and Carroll, K.C., 2019, Quantifying disconnection of groundwater from managed-ephemeral surface water during drought and conjunctive agricultural use: *Water Resources Research*, v. 55, no. 7, p. 5871–5890, accessed May 17, 2023, at <https://doi.org/10.1029/2019WR024941>.
- Griffiths, D.J., 1999, *Introduction to electrodynamics*, (3d ed.): PrenticeHall Inc., New Jersey, 576 p.
- Groundwater Management Area 14, 2016, Desired future conditions explanatory report: prepared for the Texas Water Development Board with assistance from Mullican and Associates, and Freese and Nichols, Inc., accessed May 17, 2023, at https://www.twdb.texas.gov/groundwater/dfc/docs/GMA14_DFCExpRep.pdf.
- Haas, A. and Revil, A., 2009, Electrical burst signature of pore-scale displacements: *Water Resources Research*, v. 45, no. 10, p. 1–6, accessed May 17, 2023, at <https://doi.org/10.1029/2009WR008160>.
- Hämmann, M., Maurer, H.R., Green, A.G., and Horstmeyer, H., 1997, Self-potential image reconstruction—Capabilities and limitations: *Journal of Environmental and Engineering Geophysics*, v. 2, no. 1, p. 21–35, accessed May 17, 2023, at <https://doi.org/10.4133/JEEG2.1.21>.
- Ikard, S.J., Teeple, A.P., Payne, J.D., Stanton, G. P., and Banta, J. R., 2018, New insights on scale-dependent surface and groundwater exchange from a floating self-potential dipole: *Journal of Environmental and Engineering Geophysics*, v. 23, no. 2, p. 261–287, accessed May 17, 2023, at <https://doi.org/10.2113/JEEG23.2.261>.

- Ikard, S.J., Teeple, A.P., and Humberson, D.L., 2021a, Gradient self-potential logging in the Rio Grande to identify gaining and losing reaches across the Mesilla Valley: *Water*, v. 13, no. 10, 1331, p. 1–23, accessed May 17, 2023, at <https://doi.org/10.3390/w13101331>.
- Ikard, S.J., Briggs, M.A., and Lane, J.W., 2021b, Investigation of scale-dependent groundwater/surface-water exchange in rivers by gradient self-potential logging—Numerical modeling and field experiments: *Journal of Environmental and Engineering Geophysics*, v. 26, no. 2, p. 83–98, accessed May 17, 2023, at <https://doi.org/10.32389/JEEG20-066>.
- Ikard, S.J., Wallace, D.S., Teeple, A.P., and Stanton, G.P., 2021c, Geoelectric survey of the Granite Gravel aquifer, Llano Uplift, central Texas, to determine locations for water wells: *Journal of Applied Geophysics*, v. 195, accessed May 17, 2023, at <https://doi.org/10.1016/j.japgeo.2021.104479>.
- Ikard, S.J., Wallace, D.S., Sievers, J.M., and Thomas, J.V., 2022, Waterborne self-potential, temperature, and conductivity logging data from the Elm Fork of the Trinity River between Lewisville Lake Dam and Frasier Dam Recreational Area, January 2022: U.S. Geological Survey data release, accessed May 17, 2023, at <https://doi.org/10.5066/P99L7C8E>.
- Ishido, T., and Mizutani, H., 1981, Experimental and theoretical basis of electrokinetic phenomena in rock-water systems and its application to geophysics: *Journal of Geophysical Research Solid Earth*, v. 86, no. B3, p. 1763–1775, accessed May 17, 2023, at <https://doi.org/10.1029/JB086iB03p01763>.
- Ishido, T., 1989, Self-potential generation by subsurface water flow through electrokinetic coupling, In: Merkle, G.P., Militzer, H., Hötzl, H., Armbruster, H., Brauns, J. (eds) *Detection of subsurface flow phenomena: Lecture Notes in Earth Sciences*, v. 27, Springer, Berlin, Heidelberg, accessed May 17, 2023, at <https://doi.org/10.1007/BFb0011635>.
- Jardani, A., Revil, A., Bolève, A., Dupont, J.P., Barrash, W., and Malama, B., 2007, Tomography of the Darcy velocity from self-potential measurements: *Geophysical Research Letters*, v. 34, no. 24, p. 1–6, accessed May 17, 2023, at <https://doi.org/10.1029/2007GL031907>.
- Jardani, A., Revil, A., Bolève, A., Dupont, J.P., 2008, Three-dimensional inversion of self-potential data used to constrain the pattern of groundwater flow in geothermal fields: *Journal of Geophysical Research*, v. 113, no. B9, p. 1–22, accessed May 17, 2023, at <https://doi.org/10.1029/2007JB005302>.
- Jardani, A., Revil, A., Barrash, W., Crespy, A., Rizzo, E., Straface, S., Cardiff, M., Malama, B., Miller, C., and Johnson, T., 2009, Reconstruction of the water table from self-potential data: A Bayesian approach: *Groundwater*, v. 47, no. 2, p.213–227, Accessed May 17, 2023, at <https://doi.org/10.1111/j.1745-6584.2008.00513.x>.
- Kalbus, E., Reinstorf, F., and Schirmer, M., 2006, Measuring methods for groundwater–surface water interactions: a review: *Hydrology and Earth System Sciences*, v. 10, no. 6, p. 873–887, accessed May 17, 2023, at <https://doi.org/10.5194/hess-10-873-2006>.
- McCallum, A.M., Andersen, M.S., Giambastiani, B.M.S., Kelly, B.F.J., and Acworth, R.I., 2013, River–aquifer interactions in a semi-arid environment stressed by groundwater abstraction: *Hydrological Processes*, v. 27, no. 7, p. 1072–1085, accessed May 17, 2023, at <https://doi.org/10.1002/hyp.9229>.
- Mueller, D.S., Wagner, C.R., Rehm, M.S., Oberg, K.A., and Rainville, Francois, 2013, Measuring discharge with acoustic Doppler current profilers from a moving boat (ver. 2.0, December 2013): U.S. Geological Survey Techniques and Methods, book 3, chap. A22, accessed May 17, 2023, at <https://dx.doi.org/10.3133/tm3A22>.
- National Weather Service, 2023a, Fort Worth/Dallas Climate Narrative—The climate of Dallas/Fort Worth, accessed May 17, 2023, at https://www.weather.gov/fwd/dfw_narrative.
- National Weather Service, 2023b, Fort Worth/Dallas NOWData—Daily data for a month, accessed May 17, 2023, at <https://www.weather.gov/wrh/Climate?wfo=fwd>.
- National Weather Service, 2023c, Fort Worth/Dallas—monthly and annual precipitation, accessed May 17, 2023, at <https://www.weather.gov/fwd/dmoprecip>.
- Naudet, V., Revil, A., and Bottero, J.Y., 2003, Relationship between self-potential (SP) signals and redox conditions in contaminated groundwater: *Geophysical Research Letters*, v. 30, no. 21, p. 1–4, accessed May 17, 2023, at <https://doi.org/10.1029/2003GL018096>.
- Nyquist, J.E., and Corry, C.E., 2002, Self-potential: the ugly duckling of environmental geophysics: *The Leading Edge*, v. 21, no. 5, p. 446–451, Accessed May 17, 2023, at <https://doi.org/10.1190/1.1481251>.
- Onsager, L., 1931a, Reciprocal relations in irreversible processes I: *Physical Review*, v. 37, no. 4, p. 405–426, accessed May 17, 2023, at <https://link.aps.org/doi/10.1103/PhysRev.37.405>.
- Onsager, L., 1931b, Reciprocal relations in irreversible processes II: *Physical Review*, v. 38, no. 12, p. 2265–2279, accessed May 17, 2023, at <https://link.aps.org/doi/10.1103/PhysRev.38.2265>.

- Oppenheim, A.V., and Schaffer, R.W., 2010, Discrete-time signal processing (3d ed.): Pearson Higher Education, New Jersey, 1108 p.
- Overbeek, J. Th. G., 1952, Electrochemistry of the double layer: Colloid and Interfacial Science I: in Irreversible Systems, H.R. Kryut (ed.), Elsevier, New York, 115–193.
- Region H Water Planning Group, 2021, Regional Water Plan: prepared for the Texas Water Development Board with assistance from Freese and Nichols, Inc., WSP USA Inc., and Ekistics Corporation, accessed May 17, 2023, at <https://www.twdb.texas.gov/waterplanning/rwp/plans/2021/index.asp>.
- Ren, J., Cheng, J., Yang, J., Zhou, Y., 2018, A review on using heat as a tool for studying groundwater–surface water interactions: Environmental Earth Sciences, v. 77, no. 22, accessed May 17, 2023, at <https://doi.org/10.1007/s12665-018-7959-4>.
- Revil, A., Pezzard, P.A., and Glover, P.W.J., 1999a, Streaming potential in porous media 1. Theory of the zeta potential: Journal of Geophysical Research Solid Earth, v. 104, no. B9, p. 20021–20031, accessed May 17, 2023, at <https://doi.org/10.1029/1999JB900089>.
- Revil, A., Schwaeger, H., Cathles, L.M., and Manhardt, P., 1999b, Streaming potential in porous media 2. Theory and application to geothermal systems: Journal of Geophysical Research Solid Earth, v. 104, no. B9, p. 20033–20048, accessed May 17, 2023, at <https://doi.org/10.1029/1999JB900090>.
- Revil, A., Ahmed, A.S., and Jardani, A., 2017, Self-potential: A non-intrusive groundwater flow sensor: Journal of Environmental and Engineering Geophysics, v. 22, no. 3, p. 235–247, accessed May 17, 2023, at <https://doi.org/10.2113/JEEG22.3.235>.
- Sheffer, M.W., and Oldenburg, D.W., 2007, Three-dimensional modelling of streaming potential: Geophysical Journal International, v. 169, p. 839–848, accessed May 17, 2023, at <https://adsabs.harvard.edu/full/2007GeoJI.169..839S>.
- Sill, W.R., 1983, Self-potential modeling from primary flows: Geophysics, v. 48, no. 1, p. 76–86, accessed May 17, 2023, at <https://doi.org/10.1190/1.1441409>.
- Slade, R.M., Bentley, J.T., and Michaud, D., 2002, Results of streamflow gain-loss studies in Texas, with emphasis on gains from and losses to major and minor aquifers: U.S. Geological Survey Open-File Report, accessed May 17, 2023, at <https://doi.org/10.3133/ofr0268>.
- Sophocleous, M., 2002, Interactions between groundwater and surface water—The state of the science: Hydrogeology Journal, v. 10, p. 52–67, accessed May 17, 2023, at <https://doi.org/10.1007/s10040-001-0170-8>.
- Stern R.J., 2019, Geology of the Dallas-Fort Worth Metropolis—A primer: Athenaeum Review, no. 2, accessed May 17, 2023, at <https://athenaeumreview.org/wp-content/uploads/2019/05/Stern-83-93.pdf>.
- Texas Water Development Board, 2019, Surface water–Trinity River Basin, accessed May 17, 2023, at http://www.twdb.texas.gov/surfacewater/rivers/river_basins/trinity/index.asp.
- Timm, F., and Möller, P., 2001, The relation between electric and redox potential—Evidence from laboratory to field experiments: Journal of Geochemical Exploration, v. 72, p. 115–127, accessed May 17, 2023, at [https://doi.org/10.1016/S0375-6742\(01\)00157-1](https://doi.org/10.1016/S0375-6742(01)00157-1).
- Trinity River Authority, 2021, Trinity River Basin Master Plan, accessed May 17, 2023, at <https://storymaps.arcgis.com/stories/435a1188d8f3425da9721308d90a7fd>.
- Turnipseed, D.P., and Sauer, V.B., 2010, Discharge measurements at gaging stations: U.S. Geological Survey Techniques and Methods book 3, chap. A8, accessed May 17, 2023, at <https://doi.org/10.3133/tm3A8>.
- U.S. Census Bureau, 2023, Quick facts—Texas, accessed February 17, 2023, at <https://www.census.gov/quickfacts/TX>.
- U.S. Geological Survey, 2014, Geologic database of Texas, accessed May 17, 2023, at <https://data.tnris.org/collection?c=79a18636-3419-4e22-92a3-d40c92ec-ed14#5.44/31.32/-100.077>.
- U.S. Geological Survey, 2019, Specific conductance: U.S. Geological Survey Techniques and Methods, book 9, chap. A6.3, p. 1–15, accessed May 17, 2023, at <https://doi.org/10.3133/tm9A6.3>. [Supersedes USGS Techniques of Water-Resources Investigations, book 9, chap. A6.3, version 1.2.].
- U.S. Geological Survey, 2023, USGS water data for the Nation: U.S. Geological Survey National Water Information System database, accessed February 17, 2023, at <http://doi.org/10.5066/F7P55KJN>.
- Valois, R., Cousquer, Y., Schmutz, M., Pryet, A., Delbart, C. and Dupuy, A., 2017, Characterizing stream-aquifer exchanges with self-potential measurements: Ground Water, v. 56, no. 3, p. 1–14, accessed May 17, 2023, at <https://doi.org/10.1111/gwat.12594>.
- Williams, C.R., 2010, Groundwater management plan of the Bluebonnet Groundwater Conservation District, accessed May 17, 2023, at https://www.beg.utexas.edu/files/content/beg/research/swr/mgmtplans/BLUEBONNET_GCD_MGMNT_PLAN.pdf.
- Winter, T.C., Harvey, J.W., Franke, O.L., and Alley, W.M., 1999, Groundwater and surface water: A single resource: U.S. Geological Survey Circular 1139, p. 1–88, accessed May 17, 2023, at <https://doi.org/10.3133/cir1139>.